

1 **Observationally constrained analysis of sulfur cycle in the marine atmosphere with NASA**
2 **ATom measurements and AeroCom model simulations**

3
4 Huisheng Bian^{1,2}, Mian Chin², Peter R. Colarco², Eric C. Apel³, Donald R. Blake⁴, Karl Froyd⁵, Rebecca S.
5 Hornbrook³, Jose Jimenez^{5,6}, Pedro Campuzano Jost^{5,6}, Michael Lawler^{5,7}, Mingxu Liu⁸, Marianne Tronstad Lund⁹,
6 Hitoshi Matsui⁸, Benjamin A. Nault^{5,6,10,11}, Joyce E. Penner¹², Andrew W. Rollins^{3,13}, Gregory Schill¹, Ragnhild B.
7 Skeie⁹, Hailong Wang¹⁴, Lu Xu^{15,16}, Kai Zhang¹⁴, and Jialei Zhu¹⁷

8
9 ¹Goddard Earth Sciences Technology and Research (GESTAR) II, University of Maryland at Baltimore County,
10 Baltimore, MD, USA.

11 ²NASA Goddard Space Flight Center, Greenbelt, MD, USA.

12 ³Atmospheric Chemistry Observations & Modeling Laboratory, National Center for Atmospheric Research,
13 Boulder, CO, USA.

14 ⁴Department of Chemistry, University of California Irvine, CA, USA.

15 ⁵Cooperative Institute for Research in Environmental Sciences, University of Colorado, Boulder, CO, USA.

16 ⁶Department of Chemistry, University of Colorado, Boulder, CO, USA.

17 ⁷NOAA Chemical Sciences Laboratory, Boulder, CO, USA.

18 ⁸Graduate School of Environmental Studies, Nagoya University, Nagoya, Japan.

19 ⁹CICERO Center for International Climate Research, Oslo, Norway.

20 ¹⁰Now at: Department of Environmental Health and Engineering, Whiting School of Engineering, The Johns
21 Hopkins, Baltimore, MD, USA.

22 ¹¹Now at: Center for Aerosol and Cloud Chemistry, Aerodyne Research, Inc., Billerica, MA, USA

23 ¹²Dept. of Atmospheric, Oceanic and Space Sciences, University of Michigan, Ann Arbor, Michigan, USA.

24 ¹³NOAA Earth System Research Laboratory, Chemical Sciences Division, Boulder, CO, USA.

25 ¹⁴Atmospheric Sciences and Global Change Division, Pacific Northwest National Laboratory, Richland, WA, USA.

26 ¹⁵Division of Geological and Planetary Sciences, California Institute of Technology, Pasadena, CA, USA.

27 ¹⁶Now at Department of Energy, Environmental and Chemical Engineering, Washington University in St. Louis,
28 Missouri, USA.

29 ¹⁷Institute of Surface-Earth System Science, School of Earth System Science, Tianjin University, Tianjin, China.

30
31 Correspondence to: Huisheng Bian (huisheng.bian@nasa.gov)

32
33 **Abstract**

34 The sulfur cycle plays a key role in atmospheric air quality, climate, and ecosystems, **such as**
35 **pollution, radiative forcing, new particle formation, and acid rain**. In this study, we compare the
36 spatial and temporal distribution of four sulfur-containing species, dimethyl sulfide (DMS),
37 sulfur dioxide (SO₂), particulate methanesulfonate (MSA), and particulate sulfate (SO₄), that
38 were measured during the airborne NASA Atmospheric Tomography (ATom) mission and
39 simulated by five AeroCom-III models to analyze the budget of sulfur cycle from the models.
40 This study focuses on remote regions over the Pacific, Atlantic, and Southern Oceans from near
41 the ocean surface to ~12-km altitude range, and covers all four seasons. These regions provide us
42 with highly heterogeneous natural and anthropogenic source environments, which is not usually
43 the case for traditional continental studies. We examine the vertical and seasonal variations of
44 these sulfur species over tropical, mid-, and high-latitude regions in both hemispheres. We
45 identify their origins from anthropogenic versus natural sources with sensitivity studies by
46 applying tagged tracers **in GEOS model** linking to emission types of **anthropogenic, biomass**
47 **burning, volcanic, and oceanic emissions**. **Our work presents the first assessment of AeroCom**
48 **sulfur study using ATom measurements, providing directions for improving sulfate simulations,**
49 **which remain the largest uncertainty in radiative forcing estimates in aerosol climate models.** In
50 general, the differences among model results can be greater than one-order of magnitude.
51 Comparing with observations, simulated SO₂ is generally low while SO₄ is high. **Using**

Deleted: 6

Deleted: 5

Deleted: 6

Deleted: 5

Deleted: 6

Deleted: 5

Deleted: ,

Deleted: from land versus ocean and

Deleted: and regions

Deleted: , and the model-observation agreement is much better in ATom-4 (April-May, 2018)

63 interactive oxidant calculation is insufficient to account for model sulfate bias. There are much
64 larger DMS concentrations simulated close to the sea surface than observed, indicating that the
65 DMS emissions may be too high from all models. The parameterization of converting DMS
66 seawater concentrations into DMS emission fluxes needs to be revisited. Anthropogenic
67 emissions are the dominant source (40-60% of the total amount) for atmospheric sulfate
68 simulated at locations and times along the ATom flight tracks at almost every altitude, followed
69 by volcanic emissions (18-32%) and oceanic sources (16-32%). Similar source contributions can
70 also be derived at broad ocean basin and monthly scales, indicating that any reductions of
71 anthropogenic sulfur emissions would have global impacts in modern times.

72 73 **1. Introduction**

74 Atmospheric sulfur species have wide-ranging environmental and health impacts. About two-
75 third of sulfur emissions come from anthropogenic activities (Chin et al., 2000); therefore,
76 considerable efforts have been made to reduce these sulfur emissions. For example, acid rain
77 occurs when sulfur dioxide (SO₂) is oxidized to form sulfuric acid and particulate sulfate (SO₄),
78 which fall to the ground with the rain (Bian et al., 1993; Grennfelt et al., 2020) and can devastate
79 aquatic ecosystems (Josephson et al., 2014; McDonnell et al., 2021). Through the competing
80 neutralization reaction of SO₄ and nitrate with NH₃ and other alkaline species, SO₄ affects
81 strongly both particulate nitrate formation (Bian et al., 2017) and aerosol pH (Huang et al., 2020;
82 Nault et al., 2021). Sulfate is a key component of particulate matter (PM), which degrades air
83 quality (Dong et al., 2018; Tan et al., 2018) and directly reflects the sun's rays (Moch et al.,
84 2022; Myhre et al., 2013). Due to its highly hygroscopic nature, sulfate aerosol affects cloud
85 physics (Boucher et al., 2013; Breen et al., 2021; Seinfeld et al., 2016) and thus indirectly
86 radiative forcing (Penner et al., 2016; Wang et al., 2021) through aerosol-cloud interactions. The
87 contribution of aerosols to atmospheric clouds and energy budget remains the largest uncertainty
88 in climate models (Gryspeerd et al., 2023; Jia et al., 2021, 2022; Klein et al., 2013; Malavelle et
89 al., 2017). Sulfate is important primarily because the atmospheric sulfate component itself
90 contributes to radiation forcing (RF) almost as much as all other major non-natural aerosol
91 components, as concluded from 16 AeroCom model results (Myhre et al., 2013). More
92 importantly, uncertainty in sulfate simulations in current climate models is a major contributor to
93 biases in aerosol optical depth (AOD, Fig. 3 in Gliß et al., 2021) and RF (Fig. 7 in Myhre et al.,
94 2013).

95
96 Unlike other major atmospheric aerosols, a significant fraction (i.e., roughly a quarter) of sulfate
97 in the atmosphere comes from marine biological emissions (Chin et al., 1996). The impact of
98 oceanic sulfate is particularly pronounced on marine shallow clouds, which are characterized by
99 low droplet number concentrations and weak updraft velocities (Rissman et al., 2004). Sulfur
100 research has also focused on the tropical upper troposphere (TUT), where the growth of new
101 aerosol particles and homogeneous nucleation involving sulfuric acid is at a maximum
102 (Williamson et al., 2019), and where deep convective transport allows a small portion of the
103 sources to reach the lower stratosphere. The resulting sulfate aerosols in the stratosphere can
104 persist for years (Holton et al., 1995). Unfortunately, the observations in the TUT region and
105 above are sparse. Acquiring atmospheric composition and its chemical/physical properties over
106 remote oceans is challenging, although satellites can often provide total column constraints of
107 aerosol optical depth.
108

Deleted: wreak havoc on

Deleted: TUT and above are

Deleted: -

Deleted: regions

113 The NASA Earth Venture Suborbital (EVS-2) Atmospheric Tomography (ATom) airborne
114 mission provided abundant measurements of gases and aerosols over the world's oceans (Hodzic
115 et al., 2020; Thompson et al., 2021). In particular, a suite of instruments integrated on the NASA
116 Douglas DC-8 jetliner (hereafter DC-8), made measurements of many important sulfur species
117 including dimethyl sulfide (DMS), SO₂, particulate methanesulfonate (MSA) and SO₄ over the
118 Pacific and Atlantic Oceans in both hemispheres and the Southern Ocean in all four seasons.
119 This comprehensive sulfur dataset provides us with unprecedented opportunities to assess sulfur
120 source, transport, chemistry, deposition, and particle activation and growth represented in the
121 global aerosol models, and to estimate the extent of anthropogenic influence on remote oceanic
122 atmospheric composition and cloud properties.

Deleted: aircraft

124 This study has two specific scientific goals. First, we explore the vertical and seasonal variation
125 of sulfur species (i.e., DMS, SO₂, MSA, and SO₄) using ATom measurements and simulations
126 from five global models that participated in the AeroCom-ATom model experiments. AeroCom
127 is an international initiative of scientists aiming at the advancement of the understanding of the
128 global aerosol and its impact on climate (<https://aerocom.met.no/>). Here we focus on remote
129 regions over the Pacific, Atlantic, and Southern Oceans, from near the surface to an altitude of
130 about 12 km, covering all four seasons. Second, we determine whether the produced SO₄
131 originated from anthropogenic or natural sources by using tagged tracers associated with
132 emission types,

Deleted: ilometers

Deleted: from land or ocean sources and

Deleted: and regions

134 Our work is the first study to use ATom measurements for comparison with the AeroCom
135 models, focusing on all sulfur species simulated in current aerosol climate models. This work
136 extends previous efforts using ATom measurements to evaluate the organic carbon (Hodzic et
137 al., 2020) and black carbon (Katich et al., 2018) of AeroCom models, as well as individual
138 models focusing on new particle formation in the tropics (Williamson et al., 2019), fine aerosol
139 lifetime (Gao al. al., 2022), aerosol vertical transport (Yu et al., 2019), sea salt (Bian et al.,
140 2019), smoke (Schill et al., 2020), mineral dust (Froyd et al., 2022), and DMS chemistry (Fung
141 et al., 2022). Furthermore, to our knowledge, there are no studies that systematically investigate
142 the changes and sources of all major sulfur species in the ocean. Our study aims not only to
143 reveal sulfur variability based on multiple measurements and model simulations, but also to tease
144 out the underlying processes behind the variability through a comprehensive analysis of
145 simulated sulfur species in aerosol climate models.

146
147 The structure of this paper is as follows. Section 2 describes the ATom measurements and the
148 AeroCom models used in this study. Section 3 presents the ATom-AeroCom sulfur comparison
149 from different perspectives, namely the overall comparison in Sect. 3.1, the vertical profiles in
150 Sect. 3.2, and the regional and seasonal analysis in Sect. 3.3. The sulfur budget analysis is given
151 in Sect. 4. We further present investigations of source origins for aerosol SO₄ along flight tracks
152 and over oceans in Sect. 5. Finally, we summarize our findings in Sect. 6.

154 2. Data

155 2.1 ATom measurements

156 ATom was a NASA-funded Earth Venture Suborbital project designed to study the effects of air
157 pollution on chemically reactive gases, aerosols, and greenhouse gases in the remote atmosphere.
158 ATom deployed a large suite of gas and aerosol measurement instruments on the NASA DC-8

163 aircraft for systematic sampling, covering an extended region of the globe from 85°N to 85°S
164 over the Pacific and Atlantic Oceans, with vertical profiles from near-surface to near-tropopause
165 (i.e., 0.2-12 km, Thompson et al., 2021). Four ATom deployments (ATom-1 to -4) were
166 executed over each of the four seasons from 2016 to 2018, and their flight paths are shown in
167 Fig. 1. The extensive aerosol and gas measurements made during ATom include inorganic and
168 organic aerosols, precursor gases, particle size distributions and particle composition. Table 1
169 lists the instruments for ATom sulfur species observations used in this study including the
170 relevant sampling details needed for the model comparison.

171 We use SO₄ and MSA that had been measured by two instruments, the University of Colorado
172 Aerodyne high-resolution time-of-flight aerosol mass spectrometer (AMS, Canagaratna et al.,
173 2007; Guo et al., 2021), and the NOAA Particle Analysis by Laser Mass Spectrometry (PALMS,
174 Froyd et al., 2019). The latter makes *in situ* measurements of the chemical composition of
175 individual aerosol particles. Furthermore, AMS measured submicron aerosols while PALMS
176 provided mass mixing ratio and size distribution up to 3 μm in dry diameter (Brock et al., 2019).
177 It is worth noting that AMS data were independently processed and reported at both 1-s and 60-s
178 time resolutions by instrument PI (Jimenez et al., 2019). The detection limit varied with different
179 averaging time resolutions, and they were provided directly for each sampling point in AMS
180 datasets. Some negative measurements were also presented in AMS datasets, and this is normal
181 for measurements of very low concentrations in the presence of instrumental noise. The AMS
182 data at 60-s resolution is recommended owing to more robust peak fitting at low concentrations
183 (Hodzic et al., 2020). Given the complex data overlays (i.e., starting, ending, and frequency)
184 reported from multiple instruments, the ATom team also provide a 10-s merged dataset to
185 facilitate users' applications. In this study, we evaluate data reported in different time
186 resolutions, using AMS as an example, to ensure the quality of merged data that are exclusively
187 used as the primary dataset in this work.

189 Two instruments were used for SO₂ measurements; the California Institute of Technology
190 Chemical Ionization Mass Spectrometer (CIMS) and the NOAA Laser Induced Fluorescence
191 (LIF) (Table 1). The CIMS uses CF₃O⁻ as a reagent ion which reacts with SO₂ via fluoride ion
192 transfer chemistry. The product ion is detected by a compact time-of-flight mass spectrometer
193 (CToF). The precision of the CIMS SO₂ measurement decreases with increasing water vapor
194 concentration (Eger et al., 2019; Huey et al., 2004; Jurkat et al., 2016; Rickly et al., 2021),
195 making it challenging to measure SO₂ in remote ocean regions. In these regions, the ambient
196 water vapor may be sufficiently high that the CIMS SO₂ precision at 1-s resolution (~130 parts
197 per trillion by volume, pptv) is insufficient for measuring ambient SO₂ value there (<100 pptv).
198 To address this shortcoming, the ATom science team added a new instrument, the NOAA LIF, to
199 the ATom-4 payload. The NOAA LIF instrument uses red-shifted laser-induced fluorescence to
200 detect SO₂ at very low ppt levels (Rickly et al., 2021; Rollins et al., 2016). Both instruments
201 report negative values and the detection limit of the LIF instrument is about 2 pptv.

203 DMS was measured during ATom by two instruments, the University of California, Irvine
204 Whole Air Sampler (WAS), and the NCAR Trace Organic Gas Analyzer (TOGA). The WAS
205 reported DMS for all four ATom deployments, while the TOGA reported data for ATom-2 to -4
206 and not for ATom-1 due to possible issues associated with the TOGA inlet (the inlet was
207 changed for ATom-2 to -4). Both instruments have comparable detection limit (1 pptv) and
208

Deleted: ~

Deleted:) (

Deleted: one

Formatted: Font: Italic

Deleted: ,

Deleted: ,

Deleted: were used for SO₂ measurements

215 accuracy (~15%). However, the sampling time interval of WAS (variable but ~180s) was longer
216 than TOGA (~120s).

218 2.2 AeroCom models

219 Five global aerosol models participated in an AeroCom-ATom model experiment
220 (<https://wiki.met.no/aerocom/phase3-experiments>): CAM-ATRAS, E3SM, GEOS, IMPACT,
221 and OsloCTM3. The experiment required all participating models to (1) conduct three-year-
222 simulations of 2016-2018 (i.e., covering the whole ATom observation period); (2) use or nudge
223 meteorological data for the simulation period; and (3) use the same pre-defined emission fields
224 for precursor gases and aerosol tracers. The suggested emissions are the Coupled Model
225 Intercomparison Project Phase 6 [Community Emissions Data System \(CEDS, Hoesly et al.,
226 2018\)](#) for anthropogenic source, daily biomass burning emission (such as The Global Fire
227 Assimilation System, GFAS), a dataset based on satellite volcanic SO₂ observations from the
228 OMI instrument on the Aura satellite (Carn et al., 2016, 2017) for outgassing and eruptive
229 volcanic emission, and DMS concentration in sea surface from Lana et al. (2011). Wind-driven
230 emissions, such as dust and sea salt, are calculated online by each model. [Table 2 summarizes
231 the detailed model characteristics and input datasets relevant to this study. It is worth noting that
232 CEDS specifies anthropogenic emissions from various sectors, including emissions from
233 shipping. The version of CEDS used in this work has emissions up to 2014 and all models use
234 2014 emission for ATom periods. Furthermore, unlike other models that use CEDS emissions,
235 the anthropogenic emissions of OsloCTM3 are obtained following Shared Socioeconomic
236 Pathways \(SSP\) under Representative Concentration Pathway \(RCP\) scenario with medium
237 radiative forcing by the end of the century \(SSP245, Fricko et al., 2017\), and the emissions are
238 interpolated to 2016 and 2017.](#) Following the experimental protocol, all models provided results
239 for all AToms except for OsloCTM3 that omitted data in ATom-4. Unlike traditional AeroCom
240 experiments that used gridded daily/monthly averaged data, modelers are required to interpolate
241 model results along flight track every 10 s (see more discussion in Sect. 3.1) using three-
242 dimensional high frequency (e.g., hourly or even less depending on the models' time step) data
243 to facilitate the comparison. It is worth noting that the models do not have any actual information
244 at 10-s time resolution, given their time steps are at least 10× greater and their spatial resolutions
245 are coarse. However, the interpolation methodology suggested here provides the best model
246 information at their current configuration to compare with aircraft measurements.

247
248 The AeroCom-ATom experiment also designed three sensitivity simulations by tracking gas and
249 aerosol emissions to anthropogenic, biomass burning, and volcanic sources to attribute the origin
250 of sulfur sources on sulfur simulations over remote oceans. These experiments were conducted
251 with the Goddard Earth Observing System (GEOS) model. The setup of the GEOS model
252 followed the experiment protocol generally, but GEOS used its own daily biomass burning
253 emissions that were derived from the Quick Fire Emissions Dataset (QFED) developed based on
254 MODIS fire radiative power and calculated in near real-time at 0.1° resolution (Darmenov and
255 da Silva, 2015; Pan et al., 2020). Emissions from biogenic sources were calculated using the
256 Model for Emissions of Gases and Aerosols from Nature (MEGAN) embedded in the GEOS
257 model.

258 2.3 Tag-tracer study in GEOS

Deleted: (CMIP6)

Deleted: (Feng et al., 2020)

Deleted: (

Deleted:)

Deleted: Table 2 summarizes the detailed model characteristics and input datasets relevant to this study.

Deleted: -

267 Tag trackers or tags are tied to sources of selected emission types and/or emission locations.
268 Such tag isolates plume from certain activities and is a powerful tool to help understand source
269 attribution or diagnose model performance at the process level. The mechanism behind this
270 technique is that each specific aerosol component in GEOS GOCART is modeled independently
271 of the other components, and the contribution of each emission type to the total aerosol mass is
272 not disturbed by the other emission types. Therefore, additional aerosol tracers can be easily
273 "tagged" to capture emission type (e.g., anthropogenic, biomass burning, etc.) and location
274 (local, regional or global scale). Tags can be multi-instantiated and computed simultaneously
275 with their baseline counterparts, thereby increasing the computational efficiency of scientific
276 research.

277
278 Tag-tracer technique in GEOS has been widely used in aerosol and gas studies (Bian et al., 2021;
279 Nielsen et al., 2017; Strode et al., 2018) and in supporting various aircraft field campaigns such
280 as Arctic Research of the Composition of the Troposphere from Aircraft and Satellites
281 (ARCTAS) and ATom. Such techniques are also adopted in other models such as GEOS-Chem
282 model (Fisher et al., 2017; Ikeda et al., 2017; Lin et al., 2020) and Community Earth System
283 Model (CESM, Butler et al., 2018).

284
285 Four tags linked to emission types of anthropogenic, biomass burning, volcanic, and marine
286 emissions were used in GEOS model to identify anthropogenic versus natural sources of sulfate,
287 and the results are discussed in Sect. 5.

288 3. ATom–AeroCom comparisons of sulfur species

289 This section presents a comparison of sulfur species between ATom measurements and
290 AeroCom model simulations. The consistency and diversity of data across remote regimes, both
291 horizontally and vertically, help us understand the effects of emissions, transport, and chemical
292 transformations, and shed light on improving the processes in models to best represent the ATom
293 observations.

294 3.1 Overall comparison

295 The overall performance of SO₄ PDF distribution observed from the AMS and PALMS
296 instruments and simulated by five AeroCom models for four ATom deployments is presented in
297 Fig. 2. Also shown in Fig. 2 are the corresponding various percentiles, namely, 0th (minimum),
298 25th, 50th (median), 75th, and 100th (maximum), and the mean for statistical analyses. The ATom
299 team provided a 10-s merged dataset deliberately by integrating data from various instruments to
300 a unified temporal resolution. We use this 10-s merged data where observations above detection
301 limit (DL) throughout the main text unless otherwise stated. When multiple instruments
302 measured the target field, only points where all instrument measured above DL values were
303 included in analysis, as AMS 10-s in red, and PALMS 10-s in grey in Fig. 2. All model results
304 were sampled mimicking flight observations (see Sect. 2.2), and only data with measurements
305 available were used in comparison. This approach ensures that model evaluation is based on
306 high-quality measurements. It is worth noting that the given statistical values in this method
307 represent more regions having high tracer concentration or mixing ratio. In the supplementary
308 material, we further give a model-observation comparison for all available measurement data
309 including negatives.

Deleted: As mentioned in Sect. 2.1, we have AMS data at three sampling intervals (i.e., 1-s, 60-s, and 10-s). The 10-s merged dataset were deliberately provided by the ATom observation team for integrating data from various instruments to a unified temporal resolution. We intend to use this dataset for investigation on regional and seasonal bases. Before applying it, however, we first evaluate the quality of the 10-s data. Previous studies (Hodzic et al., 2020) indicated measurement precision improved with the square root of the number of sampling points. In other words, averaging data over a 60-s interval is better than averaging over 1-s or 10-s intervals because there are more sample points in a 60-s interval. This also applies to the detection limit (DL) as it is just 3 times the precision. DL flags are assigned to convey semi-quantitative information when sampling conditions are beyond the instrument detection range and the measurements are not quantifiable. Despite the differences, the three PDFs of AMS SO₄ (red, using all relevant data including negatives) are nearly identical. Statistical analyses were further performed on the AMS 60-s, 10-s, and 1-s data sets by (1) all sampling points, even negative values, as indicated by the dot-dash box-and-whisker (approach 1), and (2) sampling points when their values exceeded DL as shown by solid box-and-whisker (approach 2). The SO₄ median (and mean) values of 60-s are closer to 10-s' but lesser than 1-s' by 0-10% in approach 1. There is slightly greater diversity (~30%, solid box-and-whisker) between these statistical values in approach 2, and the data in 60-s and 10-s are also relatively close, with a difference less than ~20%. These comparisons of the PDFs with noise and signal tell us that, on average, SO₄ is high enough in the ATom background to be unaffected by noise at any resolution. A similar analysis (not shown here) of SO₂ and DMS measurements also showed agreement between the 10-s interval dataset and the original dataset. Thus, the use of the 10-s data is acceptable in our study, given the significant differences in tracer statistics between model simulations and between model and observation.

Deleted: orange

Deleted: The observed and simulated PDF distributions are presented separately in Fig. 2.

355 The mean of PALMS SO₄ is generally about 10-50% higher than AMS SO₄ across four ATom
356 deployments. This performance may be attributed, at least in part, to the fact that the sample size
357 range of PALMS (~3 μm) is larger than that of AMS (~0.75 μm), as mentioned in Sect. 2.1.
358 However, the difference between the two observations is much smaller than the difference
359 between observation and model. Clearly, the differences in simulated SO₄ among models are
360 high and can easily exceed several orders of magnitude. Most observed and simulated SO₄
361 exhibit highest probability density around SO₄ values of 10-100 ng sm⁻³. With the exception of
362 GEOS and CAM-ATRAS, the model SO₄ PDFs show higher tails beyond 100 ng sm⁻³, which
363 explain the higher median and mean SO₄ simulated by the models. Statistical analysis performed
364 on selected percentiles (box-and-whisker panels in Fig. 2) indicates that multi-model SO₄
365 medians are about 3.7 (ATom-1), 2.2 (ATom-2), 1.9 (ATom-3), and 1.2 (ATom-4) times higher
366 than observed. In general, nearly all measurements and models indicate that SO₄ concentrations
367 on a global ocean basis are highest during the Northern Hemisphere (NH) spring season (ATom-
368 4). Similar analysis was also performed on all (e.g., both positive and negative) measurement
369 data (Fig. S2), the median/mean values of observations are naturally smaller than those in Fig. 2
370 by 8-20%, but the PDF distributions are almost identical between the two treatments.

371 Figure 3 shows the PDF distribution and statistics for SO₂. All observed and simulated data were
372 reprocessed by including points above the detection limit (2 pptv) only. Both instruments (CIMS
373 and LIF) were deployed during ATom-4. Despite CIMS being less precise than LIF (Rollins et
374 al., 2016), both instruments agreed within 95% and CIMS measured SO₂ concentrations were
375 consistently 3-7% lower than LIF measurements. This difference is within the combined
376 uncertainties of the two measurements, but it suggests a systematic calibration difference, that is
377 currently unresolved (Rickly et al., 2021). Meanwhile, the width of CIMS SO₂ PDF (measured at
378 half-height) is narrower in ATom-4 than ATom-3, because of improved measurement precision
379 in ATom-4. The CIMS resolution was improved in ATom-4, which enables a better separation of
380 SO₂ and formate-H₂O. The CIMS SO₂ PDF in ATom-4 is around 10 pptv and is more consistent
381 with LIF measurements and model simulations. In contrast, the distribution of SO₂ measured by
382 CIMS during ATom-1 to -3 is spread much wider than the models. Throughout ATom periods,
383 models, especially E3SM, GEOS, and OsloCTM3, show higher peak heights and narrower peak
384 widths. Statistics indicate lower model SO₂ medians than observed (box-and-whisker in Fig. 3),
385 especially during ATom-1. However, the model means are comparable or even higher than those
386 observed, indicating that the models simulate unobserved episode events. Consequently, the
387 simulated mean/median ratio is higher than the observed value. Among the four ATom
388 deployments, ATom-4 has much better model observation consistency. Figure S3 presents the
389 corresponding analysis, including the measured negative values. Compared to Fig. 3, the
390 observed median and mean values drop substantially (up to 50%), but the model statistics change
391 relatively small.

392
393
394 Atmospheric DMS observations are scarce, especially on a global scale. Thus, DMS
395 measurements by the two instruments (WAS and TOGA) during the four ATom deployments
396 provide an unprecedented opportunity to investigate biological DMS over global remote oceans
397 and evaluate model DMS simulations on spatial and temporal distributions. By excluding points
398 with measured values below detection limit (i.e., 1 pptv), the overall DMS comparison in Fig. 4
399 indicates TOGA has higher data peaks and probability densities when DMS ranges from 3-10
400 pptv. However, this does not appear to be consistent with the lower median and mean values of

Formatted: Subscript

Deleted: Clearly, the diversity among model simulated SO₄ is high. Although the mean of PALMS SO₄ is generally about 10-50% higher than AMS SO₄, this difference is much smaller than the difference between models that can easily exceed several orders of magnitude. The lower SO₄ of AMS than PALMS may be due at least in part to the fact that the sample size range of AMS (~0.75 μm) is smaller than that of PALMS (~3 μm), as mentioned in Sect. 2.1.

Deleted: lowest (or highest) during the Northern Hemisphere (NH) summer (or spring) season.

Deleted: 1

Deleted: error

Deleted: in one or both instruments

Formatted: rynqvb, Font: (Default) Times New Roman, (Asian) Times New Roman, 12 pt, Font color: Auto,

Deleted: Meanwhile, the width of CIMS SO₂ PDF (measured at half-height) is narrower in ATom-4, with peak heights around 10 pptv and is more consistent with LIF measurements and model simulations. In contrast, the distribution of SO₂ measured by CIMS during ATom-1 to -3 is spread much wider than the models. This wider distribution needs to be examined given the degree of seasonal variation in the SO₂ PDF. CIMS adjusted its CToF between ATom-3 and -4 to improve resolution, and thereafter managed to fit SO₂ and formate-H₂O independently, which was practically impossible for ATom-1 to -3. ...

Deleted: and higher simulated mean/median ratios than those of observations (see corresponding values given in the figure). The model-observation agreement is much better in ATom-4 among the four ATom deployments.

Deleted: 2

431 TOGA, indicating a higher tail in the WAS DMS PDF. Likewise, although the peak of WAS
 432 DMS PDF is significantly higher than all models from 3-10 pptv (~5-20 pptv for ATom-3), the
 433 median and mean of the WAS DMS are lower, suggesting an even higher tail in model DMS
 434 PDF. Overall, there is a big gap between the WAS and TOGA DMS measurements, and both are
 435 surprisingly low compared to the models. Statistical analysis performed on selected percentiles
 436 (the box-and-whisker) indicates that multi-model DMS medians are about 4.9 (ATom-1), 8.6
 437 (ATom-2), 6.6 (ATom-3), and 7.7 (ATom-4) times higher than observed, while model GEOS has
 438 a better performance (i.e., 1.2, 2.7, 2.3, and 2.8 correspondingly). Even though the model DMS
 439 median is mostly higher than the observed value, the degree of overestimation is not as serious as
 440 the mean value that can be more than tenfold, indicating a few points are simulated with
 441 extraordinarily high DMS values. Based on what we know about DMS sources and sinks, these
 442 very large simulated DMS appear most commonly in the boundary layer (BL). Indeed it is
 443 confirmed in Fig 5, by looking at the ratios of DMS median values between model simulations
 444 and observations. The analyses are performed on four vertical ranges (e.g., the entire vertical
 445 column, the BL 0-1.5 km, the low-middle free troposphere 1.5-6 km, and the upper troposphere
 446 6-12 km). The last column “MMM/MOM” refers to multi-model median to multi-observation
 447 median. The high ratio stems mostly from the BL, above which the consistency is much better.
 448 Meanwhile, the PDF distribution and statistics of the models agree better with the WAS
 449 measurement than with the TOGA measurement. We should also acknowledge that this is a very
 450 limited set of observations we used here, and that there are some longer-term DMS observations
 451 near the surface that were used as input for the parameterization of DMS emissions. More DMS
 452 observations near the ocean surface are needed to make a confident comparison.

3.2 Vertical profiles

455 Vertical profiles of ATom-1 to -4 for observed and modeled SO₄, SO₂, DMS, and MSA are
 456 shown in Figs. 6-9, respectively, for five latitude bands (from the north to the south) and for both
 457 the Pacific and Atlantic Ocean basins. Again, the profiles include equal amounts of data for each
 458 measurement and model result. In other words, all comparisons show only available points
 459 where the two observed values (i.e., AMS vs. PALMS for SO₄ and MSA, CIMS vs. LIF for
 460 SO₂, and TOGA vs. WAS for DMS) are greater than their detection limits, and where the model
 461 values are extracted.

463 The average and range of sulfur tracers for ATom-1 to -4 are shown in Figs. 6-9 and their
 464 corresponding details in each ATom are further given in Figs. S5-8. As shown in Fig. 6, the SO₄
 465 measured by the two instruments are close to each other and lie generally within the span of
 466 modelled SO₄ throughout the ATom periods. The spread of modeled SO₄ concentrations is large,
 467 easily exceeding an order of magnitude, especially in the upper troposphere. Despite the need for
 468 improvements, the models are generally able to capture the shape of the SO₄ profile.
 469 Specifically, CAM-ATRAS and GEOS have good SO₄ vertical gradients over the tropical and
 470 NH oceans, but their SO₄ values are too low compared to measurements over the Southern
 471 Hemisphere (SH) free troposphere. The SO₄ of IMPACT and OsloCTM3 decreases too slowly
 472 with altitude, as shown by their overestimated SO₄ values at high altitudes globally. E3SM,
 473 performed SO₄ simulations among other models. However, the performance of these models’
 474 SO₄ vertical profiles cannot simply be explained by the way the oxidant is applied, because
 475 among the five models, CAM-ATRAS, IMPACT, and OsloCTM3 used interactive oxidant
 476 calculations, while E3SM and GEOS used archived oxidant data (Table 2). The complexity of

Deleted: 4c,f,i,l

Deleted: Apparently, t

Deleted: ¶

DMS measurement is uniquely having a fraction of measured values in “-888”. An instrument typically has an operational detection range, which is defined by the lower limit of detection (LDL) and upper limit of detection (UDL). The flag for measured value less than the LDL is “-888” for TOGA and WAS data used in this study. The number of “-888” is not meaningless. It means that we know the value of a given measurement is below a known quantity, but we are not able to quantify that value precisely. Fig. S3 shows a similar DMS PDF analysis as Fig. 4, but instead of excluding the “-888” measurements, these are replaced with “0” as suggested by the instrument PIs. The percentage (P) of the measured “-888” is given for TOGA and WAS measurement data in the figure. These Ps for all AToms range 65% - 91%, which means majority of measured values are below LDL and the medians of both TOGA and WAS data are zero. Correspondingly, the multi-model average median (0.22, 1.13, 1.10, and 1.34 pptv for ATom-1 to -4 respectively) are much lower than those in Fig. 4. The ratio of means between model and observation for all AToms is 9.1 in Fig. S3, which is ~44% higher than 6.3 in Fig. 4. ¶

Deleted: 5

Deleted: 8

Deleted: 5

Deleted: 8

Deleted: 4

Deleted: 7

Deleted: 5

Deleted: that

Deleted: are needed

Deleted: generally

Deleted: These five models can generally be divided into three groups according to their SO₄ vertical profiles: 1. CAM-ATRAS and GEOS, 2. E3SM, and 3. IMPACT and OsloCTM. Over tropical and northern hemisphere oceans, Group 1 captures the SO₄ vertical profile well, while Group 3’s vertical profile does not decrease enough at higher altitudes. The CAM-ATRAS model recently reported an improvement of aerosol wet scavenging processes, which allow efficient removal of aerosols by convective clouds and precipitation in the tropical and mid-latitude troposphere, while trace gases such as SO₂ to reach the upper troposphere (Liu and Matsui’s 2021). In the free troposphere at high southern latitudes, SO₄ is too low for Group 1 and too high for Group 3. Group 2 (i.e.,

Deleted:)

Deleted: has

Deleted: between the

Deleted: two groups

530 the chemistry deserves more attention. Of the five models, OsloCTM3 and GEOS participated in
531 the multi-model OH assessment (Nicely et al., 2000) and OsloCTM3 had a shorter methane
532 lifetime (relative to OH) than GEOS.

533
534 Figure 7 shows generally lower modeled SO₂ volume mixing ratios compared to the CIMS
535 observations for most altitudes and latitude bins. The spread among modeled SO₂ values exceeds
536 an order of magnitude around the measured SO₂. SO₂ is better simulated by model IMPACT in
537 the NH and by models CAM-ATRAS and OsloCTM3 in the SH than other AeroCom models.
538 The tropical Pacific appears to be an interesting region, with all models except GEOS failing to
539 capture observed local SO₂ sources. Basically, the observed SO₂ is high at the surface, falls
540 rapidly in the BL, and then gradually decreases above the BL, except for ATom-1, during which
541 a second peak appears just above the BL (see Fig. S6 for the details of ATom-1 to -4 separately).
542 These observations indicate a strong local source for SO₂ in all seasons and a transport source in
543 the low free-troposphere NH summer (ATom-1). Like observations, the model GEOS provides a
544 local source for SO₂ at the surface, but it misses the plume above the BL in ATom-1, and its
545 vertical SO₂ convection is consistently too weak. Since only one flight was in ATom-1, more
546 observations are needed to confirm whether GEOS has been failing to catch the plume there
547 during the NH summer. All other models show lower SO₂ at the surface than in the lower free
548 troposphere, which is inconsistent with the observed profiles. Figure S6 also shows an excellent
549 agreement of SO₂ profiles measured by the CIMS and LIF during ATom-4 and models agree
550 with measurements better in ATom-4 as well.

551
552 DMS measurements fill in another piece of the puzzle for the atmospheric sulfur budget. As
553 shown in Fig. 8, all five AeroCom models generally overestimate DMS in the BL, particularly
554 for models CAM-ATRAS and OsloCTM3. This large bias close to the surface requires us to
555 revisit the DMS emissions employed in our models. Of the five models, DMS emissions of
556 E3SM, and IMPACT are derived directly from climate emission inventories, while the DMS
557 emission of the other three models are parameterized using monthly climatological DMS
558 concentrations in sea water and surface meteorologies (e.g. surface wind and temperature, see
559 details in Table 3). Specifically, the parameterization used to convert DMS seawater
560 concentrations into DMS emission fluxes was using Nightingale et al. (2000) in CAM-ATRAS
561 and OsloCTM3 and Liss and Merlivat (1986) in GEOS. The three models used two inventories
562 of monthly DMS seawater concentrations, Lana et al. (2011) for CAM-ATRAS and GEOS, and
563 Kettle and Andreae (2000) for OsloCTM3. It is worth noting that even the latest climatological
564 database by Lana et al. (2011) was constructed by compiling measurements before 2000, so the
565 potential long-term change of DMS emission caused by environment change could be missed
566 (Barford, 2013). Also, although the data used by Lana et al. (2011) is large (i.e., ~47,000
567 seawater concentration measurements), interpolation and extrapolation techniques were still
568 necessary in creating a global monthly climatological DMS emission. Gali et al. (2018) reported
569 updated oceanic DMS levels on a global scale using remote sensing satellite data. However,
570 much effort is still needed to accurately establish global rates of change in order to create global
571 DMS emissions for climate modeling. This parameterization of air-sea exchange is important
572 because CAM-ATRAS and OsloCTM3, using the same parameterization but different DMS
573 seawater concentrations, reported close emissions in Sect. 4. On the other hand, the DMS
574 emissions of CAM-ATRAS are almost twice as high as those of GEOS. This difference in

Deleted: , but

Deleted: Southern Hemisphere (

Deleted:)

Deleted: where

Deleted: need to improve SO₂ simulations from the surface to 400mb. ...

Deleted: 5

Formatted: Subscript

Deleted: All other models miss the strong local source and simulate SO₂ transport in the low free-troposphere, which is only shown to a lesser extent in ATom-1 observation.

Deleted: 5

Deleted: Modeled SO₂ volume mixing ratios are generally lower compared to the CIMS observations for most altitudes and latitude bins in ATom-1 to -3, which may be partially owing to the CIMS measurement issue discussed in Sect. 3.1. ...

Deleted: 7

Deleted: In

Deleted: se

Deleted: from

Deleted: CAM-ATRAS,

Deleted: directly

Deleted: s

Deleted: monthly climatological DMS concentrations in ocean water (Lana et al., 2011) and modeled sea surface wind and temperature. OsloCTM3 oceanic DMS is parameterized as in Nightingale et al. (2000). The parameterization converts the monthly DMS ocean concentration, which is taken from Kettle and Andreae (2000), a climatology based on observations, to a flux based on wind speed from the meteorological data.

Deleted: to

Deleted: e

Deleted: ,

609 emissions results from different parameterizations in the two models, since both models read the
610 same DMS seawater concentration.

611
612 Meanwhile, the modeled DMS vertical gradient is generally steeper than the observed one (e.g.,
613 Fig. 8 A54N-90N), implying slower vertical transport or faster chemical conversion of DMS to
614 SO₂ in the model. The data collected from the AeroCom models did not provide us with enough
615 information to obtain the determinants. Currently, GEOS and OsloCTM3 account for two
616 products from the oxidation of DMS (i.e., SO₂ and MSA) but only GEOS output MSA results.
617 The other models consider DMS oxidation products only as SO₂. These chemical processes in
618 the model may also need to be revisited. Previous studies proposed other chemical reactions for
619 DMS loss in the atmosphere. For example, halogen chemistry represented 71% of the DMS loss
620 in the study of Hoffmann et al. (2016). Veres et al. (2020) estimated that about 30% of DMS in
621 the atmosphere was oxidized to a sulfur compound, hydroperoxymethyl thioformate (HPMTF),
622 reported only in ATom-4. To this end, the HPMTF serves as a new reservoir of oceanic sulfur
623 and its life cycle in the atmosphere is unknown. The new finding indicates that important
624 components of Earth's sulfur cycle are not yet been fully understood and urges us to reassess this
625 fundamental marine chemical cycle. However, including these chemical DMS losses further
626 reduces DMS above the surface, making DMS in the models even lower at high altitudes.

627
628 Of the five models, only GEOS reports MSA (Fig. 9). The GEOS MSA matches observations in
629 the lower troposphere. In the upper troposphere (UT), the GEOS MSA tends to decrease slowly
630 or even increase with altitude. These patterns do not agree with observations, and this
631 inconsistency can be explained at least partially by the MSA phase stages defined in the model
632 and observations. AMS and PALMS only measure the particle phase of MSA, but GEOS MSA
633 is the total MSA and is not accurately represented by observations, especially in UT. Yan et al.
634 (2019) reported that the ratio of MSA to SO₄ can be reduced by 30% when calculations do not
635 consider methanesulfonic acid in the gas phase (MSAg) at low temperatures.

636 3.3 Regional and seasonal analysis

637 In order to analyze model performance on a regional and seasonal basis, Figs. 10-12 show
638 histograms of SO₄, SO₂, and DMS concentrations as a function of altitude (rows) and latitudinal
639 band (columns). Only multi-model median is shown here to highlight any common problems in
640 the models. Further details of each individual model are given in Figs. S2-11 and discussed in
641 supplementary material. Each model in this study has its anomalous behavior at a specific time
642 and location. With this knowledge, modelers can further explore the simulation to identify
643 potential causes of model anomalies.

644
645 High SO₄ concentration regions vary across seasons (Fig. 10). In the free troposphere (i.e., 1.5 –
646 12 km), these regions cover the tropics to mid-latitudes in summer and winter (i.e., ATom-1 and
647 ATom-2) and shift to mid- to high-latitudes in spring and autumn (i.e., ATom-3 and ATom-4).
648 The most high concentration areas appeared in the SH high-latitudes during ATom-3 (SH spring)
649 and the NH high-latitudes during ATom-4 (NH spring). Things are a bit more complicated in the
650 BL, but the tropical atmospheric SO₄ concentration appears to be always elevated, and SO₄
651 concentration levels and SO₄ interregional variation are more pronounced in ATom-1 (NH
652 summer). Among all AToms, the performance of the model SO₄ simulation is best for ATom-4
653 and worst for ATom-1 (NH summer). Compared to observations, model tends to simulate higher
654

Deleted: tease out

Deleted: ,

Deleted: 8

Deleted: behaviors are inconsistent with

Deleted: Further analyses on regional and seasonal basis are given in Figs 9-11 for SO₄, SO₂, and DMS, respectively.

Deleted: 8

Deleted: 0

Deleted: 9

Deleted: -

Deleted: Compared to observation, the free tropospheric atmosphere simulated by the models tends to be more polluted. ...

668 SO₄ concentrations in the free tropospheric atmosphere. Both observations and simulations show
669 that the SO₄ in the Pacific is higher than that in the Atlantic during the NH high-latitude autumn
670 (ATom-3) and the NH mid-latitude spring (ATom-4). The differences between observations and
671 simulations are generally larger in the Atlantic than in the Pacific, particularly in the SH. SO₄
672 concentration levels in simulated and observed worlds can differ significantly in certain areas of
673 each ATom. Differences may be caused by majority models or a few individual models. For
674 example, in summer and winter, the CAM-ATRAS model gave the highest estimates of
675 atmospheric SO₄ in the oceanic BL, but the IMPACT and OsloCTM3 models gave the highest
676 estimates of atmospheric SO₄ in the free troposphere (Fig. S9). All models except the GEOS
677 model generally overestimate SO₄ in the atmosphere.

678
679 Atmospheric SO₂ (Fig. 11) is most abundant in the BL of NH mid-latitude Pacific Ocean during
680 ATom-1 (NH summer) and the tropical Pacific BL during ATom-3 (NH autumn), and this high
681 SO₂ region extends to the atmosphere above. Areas where free tropospheric SO₂ concentrations
682 are relatively large do not necessarily follow the example of the BL. For instance, free
683 troposphere appears to be more polluted than other regions in the NH Pacific during ATom-2
684 and in the SH mid-latitude Atlantic (A40S-20S) during ATom-4, but not in the BL, implying a
685 potential source of horizontal transport. The interregional variation of SO₂ in BL is much larger
686 than in the free troposphere, from which local oceanic sources of SO₂ can be inferred. In terms of
687 model-observation comparison, model simulated SO₂ in the free troposphere is generally lower,
688 which is opposite to the case of SO₄. A rapid SO₂ to SO₄ chemical conversion in models could be
689 one of reasons. Fig. S10 further shows individual model SO₂ simulation. For example, the
690 E3SM model gives significantly higher SO₂ compared with the measurements and other models
691 in BL (Fig. S10). Unlike the case of SO₄, all models tend to underestimate SO₂ in the free
692 troposphere, with some exceptions, such as the GEOS model for the mid- to high-latitude North
693 Pacific winter (ATom-2) and the CAM-ATRAS and IMPACT models for the mid-latitude South
694 Atlantic autumn (ATom-4).

695
696 Surface DMS (Fig. 12) is generally higher in the tropics when the ocean is warm and in mid-high
697 latitudes during springtime (e.g., ATom-3 SH spring and ATom-4 NH spring). A remarkable
698 pattern of high model DMS values in the BL is revealed throughout the ATom cycle. This
699 phenomenon also occurs in the free lower troposphere, but not necessarily in the upper
700 troposphere. The high model DMS in BL can be attributed to (1) too high DMS emission, (2) too
701 slow DMS chemical loss, and (3) too slow DMS vertical transport from BL to free troposphere.
702 Additional insight can be obtained by focusing on remote high-latitudes, for example SH high-
703 latitude (40°S-70°S) Pacific, where land source impacts are limited. Thus, the higher simulated
704 SO₂ there in the BL in SYom-4 ruled out a chemical cause due to low DMS loss. The extremely
705 high surface DMS is also not due to the slow vertical transport because simulated DMS is also
706 high in the layers above the BL. A large model DMS emission is likely responsible for the
707 simulated high surface DMS. The overestimation of surface DMS multi-model median in Fig. 12
708 is clearly attributable to the contribution of all models shown in Fig. S11, with the models CAM-
709 ATRAS and OsloCTM3 being more prominent.

710 4. Sulfur budget from AeroCom models

711 Budget analysis is a simple and basic method that has been widely used to document the
712 underlying performance of a model. This analysis allows us to evaluate the AeroCom-III sulfur
713

Deleted: , and more discussion is given in the Supplement.

Deleted: 0

Deleted: pollution affects

Deleted: pollution is relatively polluted

Deleted: free troposphere appears to be more polluted than other regions

Deleted: in

Deleted: 1

Deleted: when the hemisphere is in

Deleted:

Deleted: , suggesting a potential slower vertical transport or faster DMS chemical loss in models

Deleted: The convoluted effort can be somehow alleviated by ...

Deleted: giving

729 [simulations against previous AeroCom-I and -II studies and reserves a record for future model](#)
730 [evaluations.](#) Table 4 summarizes the global sulfur budgets for emissions, wet/dry deposition and
731 chemistry from the five models. Clearly, the largest source of sulfur (~70 TgS/yr) is SO₂ emitted
732 directly from anthropogenic (~78%), biomass burning (~2%), and volcanic sources (~20%).
733 Biogenic DMS (~15-30 TgS) produced and outgassed from decomposition of marine organic
734 molecules provides the largest natural source of sulfur to the atmosphere. A small amount of SO₄
735 (< 3%) is emitted directly from anthropogenic sources.

Deleted: 3

Formatted: Subscript

Formatted: Subscript

736
737 DMS is oxidized in the atmosphere by OH and NO₃ radicals to form SO₂ and MSA. This
738 biological source of SO₂, along with SO₂ emitted directly from other sources, reacts with
739 hydroxyl radicals (OH) in the gas phase and hydrogen peroxide (H₂O₂) and ozone (O₃) in the
740 aqueous phase to produce sulfuric acid (H₂SO₄) and eventually sulfate particles, which play an
741 important role in the formation of clouds over the oceans.

742
743 In the five models, DMS has the shortest global average lifetime (0.6-2.0 days), followed by SO₂
744 (1.1-1.8 days), and SO₄ the longest lifetime (3.1-5.6 days). Among them, GEOS has the lowest
745 global burden and shortest lifetime for all sulfur species. The magnitudes of global burdens and
746 lifetimes shown here support the model performance shown in Figs. 2-8. For example, models
747 CAM-ATRAS and OsloCTM3 emit highest DMS, which is consistent with the highest DMS
748 value (Fig. 4 and S11) and longest lifetime simulated by the two models.

Deleted: 0

749
750 The key budget items include DMS emission, SO₂ emission, sulfate source or total deposition
751 (source and deposition are pretty much the same as [expected](#)), lifetime (reversely proportional to
752 the loss rate), and total atmospheric mass load. From the multi-model mean and standard
753 deviation, the “diversity” can be calculated. Figure 13 shows the global mean budget items in the
754 percentage deviation of each model from the multi-model mean, following the same concept
755 shown in Schulz et al. (2006) and Gliss et al. (2021). It reveals the processes causing model
756 differences. For example, E3SM and GEOS have approximately the same SO₂ emissions and
757 total sulfate sources, but the sulfate lifetime is much shorter in GEOS (implying faster removal
758 rates) thus smaller sulfate burden that is consistent with lower sulfate concentrations in GEOS
759 than in E3SM. At the same time, the lower total sulfate source in E3SM is compensated by
760 longer lifetime compared to CAM-ATRAS, resulting in a comparable global burden of SO₄ in
761 the two models.

Deleted: they should be

Deleted: 2

Deleted: ,

Deleted: ,

762
763 It is worth pointing out that the much lower atmospheric SO₄ mass loading of the GEOS
764 simulations is not necessarily related to the poor performance of the GEOS SO₄ simulations, as
765 revealed by the model-measurement comparison in Figs 2, 6, and S9. Although the multi-model
766 mean (or median) often represents the best simulation in the modeling domain, common
767 modeling problems or too small model sample can compromise this effort.

Deleted: 5

Deleted: 8

768
769 [To date, there have been no sulfur budget reports focusing on the vast ocean. However, previous](#)
770 [AeroCom studies have reported global sulfate atmospheric loading and its diversity across](#)
771 [multiple AeroCom models using monthly and global mean column loadings. Table 5 summarizes](#)
772 [these studies, including their reported global and annual sulfate multi-model mean \(MMM\) and](#)
773 [diversity \(\$\delta\$ \). \$\delta\$ is related to the standard deviation \(`std_dev`\) and is defined as \$\delta = \text{std_dev} /\$](#)
774 [MMM *100 \(%\). The results of this work are lower than AeroCom-I but higher than AeroCom-](#)

783 II, which may be related to the different target years involved in these studies. One point to note
784 is that the diversity δ of AeroCom-III models has not reduced since AeroCom-I, which was
785 studied nearly 20 years ago.

787 5. Source origins for aerosol SO₄ along flight track and Ocean basins

788 In this section, we perform an analysis of source attribution by tagging the sulfur source types
789 using the GEOS model. This model is the only one that provides tagged data. Our goal is to
790 understand the sources (anthropogenic, biological, volcanic) of sulfate aerosols in remote regions
791 and how chemistry, transport, and removal processes determine the vertical distribution of
792 sulfate aerosols across seasons and ocean locations.

793
794 Figure 14a presents a quantitative summary of the source attribution of aerosol SO₄ sampled
795 along the ATom flight tracks. The analysis was performed over four seasons, spanning the
796 troposphere and three vertical layers (i.e., marine boundary layer, free troposphere and upper
797 troposphere). Overall, anthropogenic emissions were the dominant source (40–60% of the total)
798 of simulated tropospheric SO₄ along the ATom flight tracks for almost all altitudes and seasons,
799 followed by volcanic (18–32%) and oceanic sources (16–32%). Anthropogenic pollution
800 prevailed over remote oceans most in spring and autumn (ATom-3 and -4). The overall
801 contributions from volcanic and oceanic sources are comparable during the ATom periods.
802 Meanwhile, the ocean source contribution has an obvious seasonal variation which is most active
803 during the SH summer (ATom-2), when marine biochemical activity in the vast Southern Ocean
804 is the largest. Volcanos show the largest contribution in the NH summer 2016 (ATom-1) during
805 the four ATom deployments. Given the irregular and character of eruptions, the volcanic
806 contribution deserves further discussion below.

807
808 In the vertical direction, SO₄ from anthropogenic emissions contributes more than 50% to the
809 free to upper troposphere. Even in the marine boundary layer, anthropogenic sources of SO₄ still
810 account for the largest fraction, except in the SH summer (ATom-2) when oceanic source
811 became dominant. The relative importance of volcanic and marine sources varies not only
812 seasonally but also vertically. Oceanic sources understandably make up a significant fraction
813 (26–42%) of SO₄ in the boundary layer. In the free troposphere, its contribution drops off
814 sharply, reflecting its local surface source characteristics. On the other hand, SO₄ from
815 anthropogenic emissions (including shipping emission) expands in the free troposphere,
816 suggesting that the source originated from distant continental areas. Volcanic SO₄ remains nearly
817 constant throughout the troposphere, making volcanoes the second largest source there.
818 Meanwhile, the contribution of others (OTH including biomass burning) to remote ocean SO₄ is
819 relatively small (< 3%) and will not be discussed further in this study.

820
821 The sources of SO₄ discussed above are deduced from the location and timing of the ATom,
822 flight path. Conclusions about the total contribution of the ocean needs caution, as there may be
823 representativeness issues using such narrow-band and instantaneous sampling. There might be a
824 situation where, for example, volcanoes provide a very large signal but only account for a small
825 measured area, and in most regions, volcanoes play a very minor role. Whereas oceanic sources
826 in the marine boundary layer perhaps were the dominant source for a much wider region but the
827 SO₄ concentration resulting from the DMS was overall a smaller amount compared to other
828 sources where near a volcanic or anthropogenic source. To address this representation issue, we

Deleted: 3

Deleted: at its most active

Deleted: event

Deleted: where and

Deleted: over

Deleted: remote oceans

Formatted

Deleted: 's

836 perform one more analysis with the model data averaged over a wider oceanic region (the shaded
837 orchid area in Fig. 1) and over a longer period (i.e., monthly mean over ATom periods). Such
838 source attributions are given in Fig. 14b.

Deleted: 3

840 Qualitative conclusions drawn from source attribution along the flight tracks generally apply to
841 the ocean basin source attribution, albeit to a slightly different extent. This confirms that
842 continental man-made sources dominate tropospheric SO₄ even over oceans. There is a clear
843 seasonal variation in oceanic contribution, which is largest in austral summer (ATom-2)
844 followed by boreal summer (ATom-1). Concerning volcanic sources, emissions from volcanoes
845 are of two types, One type is the volcanic degassing emissions that tend to remain nearly
846 constant throughout the year and are equivalent to about 20% of SO₂ global anthropogenic
847 emissions. This degassing emission ensures that volcanoes contribute more than 20% to SO₄
848 over the oceans. The other type consists in the volcanic eruptions. Due to the irregularity of
849 volcanic eruptions in terms of different eruption locations, magnitudes, and times, volcanic
850 eruptions can cause severe fluctuations in SO₄ in the atmosphere. Compared with the source
851 attribution along the flight trajectory, the volcanic contribution decreased over a larger spatial
852 and temporal domain (i.e., ocean basin and monthly mean) in the NH winter 2017 by 32%
853 (ATom-2) and increased in all other three seasons by 14-33%, especially in the NH spring 2018
854 (ATom-4), when the massive Kilauea eruption in Hawaii began on 3 May 2018. Contrarily, the
855 anthropogenic contribution increased in the NH winter (ATom-2) by 5% and decreased in other
856 seasons by 7-21%.

Deleted: It has

Deleted: There are two types of volcanic emissions

Deleted: v

Formatted: Font: 12 pt

Deleted: explosive

857 6. Conclusions

859 This study investigates sulfur in remote tropospheric regions at global and seasonal scales using
860 airborne ATom measurements and AeroCom models. The goal is to understand the atmospheric
861 sulfur cycle over the remote oceans, each model's behavior and the spread of model simulations,
862 as well as the observation-model discrepancies. Such understanding and comparison with real
863 observations are crucial to narrow down the uncertainty in model sulfur simulation. Even after
864 decades of development, models are still struggling to accurately simulate sulfur distributions,
865 with differences between models often exceeding an order of magnitude. On the other hand, the
866 agreement between instruments is usually much better. Differences between modeled SO₄ are
867 particularly large in the tropical upper troposphere, where deep convective transport allows a
868 small portion of sulfur sources to reach the lower stratosphere where resultant sulfate aerosols
869 can persist for many years. Compared with observations, simulated SO₂ is generally low while
870 SO₄ is high. Modeled DMS values are typically an order of magnitude higher than observed
871 DMS near the surface, pointing to a need to revisit the DMS emission inventories and/or the
872 biogeochemical modules used to predict DMS emissions. Our work also suggests investigating
873 three other potential corresponding processes: whether the chemical conversion from SO₂ to SO₄
874 is too rapid, whether DMS-generated free tropospheric SO₂ is too low, and whether the vertical
875 transport of DMS and SO₂ from BL to free troposphere is too low. This further investigation
876 requires atmospheric oxidant fields and the ability to track SO₂ production and loss using tagged
877 tracers.

Deleted: , and the model-observation agreement is much better in ATom-4

879 We investigate source attribution of SO₄ over remote oceans seasonally and vertically. Sampled
880 at the location and time of ATom measurements, anthropogenic emissions were the dominant
881 source (40–60% of the total) of simulated tropospheric SO₄ at almost all heights and seasons,

889 followed by volcanic (18–32%) and oceanic sources (16–32%). These contributions changed to
890 34–56%, 17–37%, and 19–37% when extended to the broad Pacific and Atlantic during the
891 months of ATom deployment. This survey confirms that anthropogenic sources dominate
892 tropospheric SO₄ even over oceans. Given that we find DMS source to be overestimated in the
893 models, the anthropogenic sources overall are a larger portion of the budget, and biogenic is
894 likely smaller than volcanic. Volcanic degassing throughout the year contributes about 20%, and
895 this proportion is increased by explosive eruptions that vary in location and timing. The oceanic
896 contribution has obvious seasonal variation, the largest in the Southern Hemisphere summer,
897 followed by the Northern Hemisphere summer.

899 It is understood that anthropogenic sulfur emissions currently offset a significant portion of
900 greenhouse gas warming, but they are rapidly declining through emissions controls. As these
901 anthropogenic emissions decrease, natural sources of sulfur, particularly bio-derived sulfur
902 compounds discharged from the world's oceans, will increase their relative contribution.
903 Therefore, more efforts are needed to understand the sulfur cycle in remote environments. On the
904 other hand, our study is the first asserting that anthropogenic emissions remain a major source of
905 sulfate aerosols generated over remote oceans during the ATom deployment periods, suggesting
906 that any limitation of anthropogenic sulfur emissions would have modern global implications.

907
908 Even after two decades of development, the diversity of sulfate simulations from AeroCom-I to
909 AeroCom-III has not decreased. However, accurate sulfate simulation in current climate models
910 is crucial to reduce radiative forcing biases. Several potential directions for improving sulfur
911 simulations are suggested above. More importantly, apart from the shortcomings of individual
912 models, all modelers should focus on the calculation of the air-sea exchange flux formula, as it
913 plays a key role in determining DMS emissions. Modelers also need to study DMS and SO₂
914 vertical transport as well as SO₄ wet deposition during long-distance transport, as model biases
915 are greatest at high altitudes. One suggestion to modelers is that the use of online oxidant fields
916 is insufficient to explain the model sulfate bias, as there was no systematic bias in the sulfate
917 simulations between the models using interactive oxidants and the models using archival
918 oxidants in this study. The complexity of chemistry deserves more attention.

920 *Code availability.* The GEOS Earth System Model source code and the instructions for model build are available
921 at <https://github.com/GEOS-ESM/GEOSgcm/> (Last accessed: 28 August 2023).

923 *Data availability.* The AeroCom model outputs needed to reproduce the results described in this paper are
924 publicly available for download at <https://acd-ext.gsfc.nasa.gov/anonftp/acd/tropo/bian/ATom-AeroCom-Sulfur/>.
925 The ATom data was obtained from their ESPO Data Archive: <https://espo.nasa.gov/atom/content/ATom>, last
926 accessed: 28 August 2022.

927 *Author contributions.*

929 BH and MC conceptualized ATom-AeroCom experiment. BH performed analysis and wrote the manuscript. BH,
930 PRC, MLi, MTL, RBS, HM, JEP, HW, KZ, and JZ provided AeroCom model results and ECA, KF, RSH, JJ, PCJ,
931 MLa, BAN, AWR, GS, and LX contributed to ATom measurements. All authors contributed to the editing of the
932 manuscript.

933 *Competing interests.*

935 At least one of the co-authors is a member of the editorial board of Atmospheric Chemistry and Physics.
936

Deleted:

Deleted:

Deleted: -

Deleted: -

Deleted: -

Deleted: from land

Deleted: shows

944 *Acknowledgements.*

945 HB, MC, and PRC acknowledge the GEOS model developmental efforts at Global Modeling and Assimilation
946 Office (GMAO). This work was supported by NASA's Aura STM and ISFM programs and ACMAP award
947 (80NSSC23K1000). The computing resources supporting this work were provided by the NASA High-End
948 Computing (HEC) Program through the NASA Center for Climate Simulation (NCCS).
949 ECA and RSH acknowledge the support of the National Center for Atmospheric Research, which is a major facility
950 sponsored by the National Science Foundation under Cooperative Agreement No. 1852977.
951 MLI acknowledges the support of JSPS Postdoctoral Fellowships for Research in Japan (Standard).
952 HM was supported by the Ministry of Education, Culture, Sports, Science, and Technology and the Japan Society
953 for the Promotion of Science (MEXT/JSPS) KAKENHI grants (JP19H05699, JP19KK0265, JP20H00196,
954 JP20H00638, JP22H03722, JP22F22092, JP23H00515, JP23H00523, and JP23K18519); by the MEXT Arctic
955 Challenge for Sustainability II (ArCS II) project (JPMXD1420318865); and by the Environment Research and
956 Technology Development Fund 2-2003 (JPMEERF20202003) and 2-2301 (JPMEERF20232001) of the
957 Environmental Restoration and Conservation Agency.
958 KZ and HW acknowledge support by the U.S. Department of Energy (DOE), Office of Science, Office of Biological
959 and Environmental Research, Earth and Environmental Systems Modeling program. The Pacific Northwest National
960 Laboratory (PNNL) is operated for DOE by Battelle Memorial Institute under contract DE-AC05-76RLO1830.
961 LX thanks Michelle Kim, Hannah Allen, John Crouse, and Paul Wennberg for operating the Caltech CIMS
962 instrument during ATom. LX acknowledges NASA grant NNX15AG61A.
963 MTL thanks Marit Sandstad (CICERO) for assistance with the model post-processing and acknowledges
964 the National Infrastructure for High Performance Computing and Data Storage in Norway (UNINETT) resources
965 (grant NN9188K).
966 RBS acknowledges funding from the Research Council of Norway (grant number 314997).

967
968 **References**

969 Abdul-Razzak, H. and Ghan, S.: A parameterization of aerosol activation, 2. Multiple aerosol
970 types, *J. Geophys. Res. Atmos.*, 105, 6837–6844, <https://doi.org/10.1029/1999JD901161>, 2000.

971 Allen, H. M., Bates, K. H., Crouse, J. D., Kim, M. J., Teng, A. P., Ray, E. A., and Wennberg, P.
972 O.: H₂O₂ and CH₃OOH (MHP) in the Remote Atmosphere: 2. Physical and Chemical Controls,
973 *J. Geophys. Res. Atmos.*, 127, e2021JD035702, <https://doi.org/10.1029/2021JD035702>, 2022.

974 Bacmeister, J., Suarez, M., and Robertson, F. R.: Rain Reevaporation, Boundary-Layer,
975 Convection Interactions, and Pacific Rainfall Patterns in an AGCM, *J. Atmos. Sci.*, 63, 3383–
976 3403, <https://doi.org/10.1175/JAS3791.1>, 2006.

977
978 Barahona, D. and Nenes, A.: Parameterizing the competition between homogeneous and
979 heterogeneous freezing in cirrus cloud formation – monodisperse ice nuclei, *Atmos. Chem.*
980 *Phys.*, 9, 369–381, <https://doi.org/10.5194/acp-9-369-2009>, 2009.

981
982 Barahona, D., Molod, A., Bacmeister, J., Nenes, A., Gettelman, A., Morrison, H., Phillips, V.,
983 and Eichmann, A.: Development of two-moment cloud microphysics for liquid and ice within
984 the NASA Goddard Earth Observing System Model (GEOS-5), *Geosci. Model Dev.*, 7, 1733–
985 1766, <https://doi.org/10.5194/gmd-7-1733-2014>, 2014.

986
987 Barford, E.: Rising ocean acidity will exacerbate global warming, *Nature*,
988 <https://doi.org/10.1038/nature.2013.13602>, 2013.

989
990 Bian, H., Luo, C., and Li, X.: Numerical modeling of air pollutant and rainfall effect on acid wet
991 deposition, *ACTA Meteorol. Sin.*, 7, 3, 273–286, 1993.

Deleted: and

Deleted: IT

Deleted:

995
996 Bian, H., Chin, M., Hauglustaine, D. A., Schulz, M., Myhre, G., Bauer, S. E., Lund, M. T.,
997 Karydis, V. A., Kucsera, T. L., Pan, X., Pozzer, A., Skeie, R. B., Steenrod, S. D., Sudo, K.,
998 Tsigaridis, K., Tsimpidi, A. P., and Tsyro, S. G.: Investigation of global nitrate from the
999 AeroCom Phase III experiment, *Atmos. Chem. Phys.*, 17, 12911–12940,
1000 <https://doi.org/10.5194/acp-17-12911-2017>, 2017.
1001
1002 [Bian, H., Froyd, K., Murphy, D. M., Dibb, J., Darmenov, A., Chin, M., Colarco, P. R., da Silva,](#)
1003 [A., Kucsera, T. L., Schill, G., Yu, H., Bui, P., Dollner, M., Weinzierl, B., and Smirnov, A.:](#)
1004 [Observationally constrained analysis of sea salt aerosol in the marine atmosphere, *Atmos. Chem.*](#)
1005 [Phys.](#), 19, 10773–10785, <https://doi.org/10.5194/acp-19-10773-2019>, Aug., 2019.
1006
1007 [Bian, H., Lee, E., Koster, R. D., Barahona, D., Chin, M., Colarco, P. R., Darmenov, A.,](#)
1008 [Mahanama, S., Manyin, M., Norris, P., Shilling, J., Yu, H., and Zeng, F.: The response of the](#)
1009 [Amazon ecosystem to the photosynthetically active radiation fields: integrating impacts of](#)
1010 [biomass burning aerosol and clouds in the NASA GEOS Earth system model, *Atmos. Chem.*](#)
1011 [Phys.](#), 21, 14177–14197, <https://doi.org/10.5194/acp-21-14177-2021>, 2021.
1012
1013 Boucher, O., Randall, D., Artaxo, P., Bretherton, C., Feingold, G., Forster, P., Kerminen, V.-M.,
1014 Kondo, Y., Liao, H., Lohmann, U., Rasch, P., Satheesh, S., Sherwood, S., Stevens, B., and
1015 Zhang, X.: in: *Climate Change 2013: The Physical Science Basis*, in: *Contribution of Working*
1016 *Group I to the Fifth Assessment Report of the Intergovernmental Panel on Climate Change:*
1017 *Clouds and Aerosols*, edited by: Stocker, T., Qin, D., Plattner, G.-K., Tignor, M., Allen, S.,
1018 Boschung, J., Nauels, A., Xia, Y., Bex, V., and Midgley, P., Cambridge University Press,
1019 Cambridge, UK and New York, NY, USA, 571–657, 2013.
1020
1021 Breen, K. H., Barahona, D., Yuan, T., Bian, H., and James, S. C., Effect of volcanic emissions on
1022 clouds during the 2008 and 2018, *Atmos. Chem. Phys.*, 21, 7749–7771,
1023 <https://doi.org/10.5194/acp-21-7749-2021>, 2021.
1024
1025 Brock, C. A., Williamson, C., Kupc, A., Froyd, K. D., Erdesz, F., Wagner, N., Richardson, M.,
1026 Schwarz, J. P., Gao, R.-S., Katich, J. M., Campuzano-Jost, P., Nault, B. A., Schroder, J. C.,
1027 Jimenez, J. L., Weinzierl, B., Dollner, M., Bui, T., and Murphy, D. M.: Aerosol size distributions
1028 during the Atmospheric Tomography Mission (ATom): methods, uncertainties, and data
1029 products, *Atmos. Meas. Tech.*, 12, 3081–3099, 2019.
1030
1031 [Butler, T., Lupascu, A., Coates, J., and Zhu, S.: TOAST 1.0: Tropospheric Ozone Attribution of](#)
1032 [Sources with Tagging for CESM 1.2.2, *Geosci. Model Dev.*, 11, 2825–2840,](#)
1033 <https://doi.org/10.5194/gmd-11-2825-2018>, 2018.
1034
1035 Carn, S. A., Clarisse, L., and Prata, A. J.: Multi-decadal satellite measurements of global
1036 volcanic degassing, *J. Volcanol. Geotherm. Res.*, 311, 99–134,
1037 <http://dx.doi.org/10.1016/j.jvolgeores.2016.01.002>, 2016.
1038

1039 Carn, S. A., Fioletov, V. E., McLinden, C. A., and Krotkov, N. A.: A decade of global volcanic
1040 SO₂ emissions measured from space, *Sci. Rep.*, 7, 44095, <https://doi.org/10.1038/srep44095>,
1041 2017.
1042
1043 Chin, M., Rood, R. B., Lin, S. J., Müller, J.-F., and Thompson, A. M.: Atmospheric sulfur cycle
1044 simulated in the global model GOCART: model description and global properties, *J. Geophys.*
1045 *Res. Atmos.*, 105, D20, 24671–24687, <https://doi.org/10.1029/2000JD900384>, 2000.
1046
1047 Colarco, P. R., da Silva, A., Chin, M., and Diehl, T.: Online simulations of global aerosol
1048 distributions in the NASA GEOS-4 model and comparisons to satellite and ground-based aerosol
1049 optical depth, *J. Geophys. Res. Atmos.*, 115, D14207, <https://doi.org/10.1029/2009JD012820>,
1050 2010.
1051
1052 Crounse, J. D., McKinney, K. A., Kwan, A., J. and Wennberg, P. O.: Measurement of Gas-Phase
1053 Hydroperoxides by Chemical Ionization Mass Spectrometry, *Anal. Chem.*, 78, 19, 6726–6732,
1054 <https://doi.org/10.1021/ac0604235>, 2006.
1055
1056 Darmanov, A. and da Silva, A.: The Quick Fire Emissions Dataset (QFED) - Documentation of
1057 versions 2.1, 2.2 and 2.4, NASA TM-2015-104606, Vol. 38, 183 pp., 2015.
1058
1059 Dentener, F., et al. (2006). "Emissions of primary aerosol and precursor gases in the years 2000
1060 and 1750 prescribed data-sets for AeroCom." *Atmospheric Chemistry and Physics* 6: 4321-4344.
1061
1062 Dong, X., Fu, J. S., Zhu, Q., Sun, J., Tan, J., Keating, T., Sekiya, T., Sudo, K., Emmons, L.,
1063 Tilmes, S., Jonson, J. E., Schulz, M., Bian, H., Chin, M., Davila, Y., Henze, D., Takemura, T.,
1064 Benedictow, A. M. K., and Huang, K.: Long-range transport impacts on surface aerosol
1065 concentrations and the contributions to haze events in China: an HTAP2 multi-model study,
1066 *Atmos. Chem. Phys.*, 18, 15581-15600, <https://doi.org/10.5194/acp-18-15581-2018>, 2018.
1067
1068 Eger, P. G., Helleis, F., Schuster, G., Phillips, G. J., Lelieveld, J., and Crowley, J. N.: Chemical
1069 ionization quadrupole mass spectrometer with an electrical discharge ion source for atmospheric
1070 trace gas measurement, *Atmos. Meas. Tech.*, 12, 1935–1954, [https://doi.org/10.5194/amt-12-](https://doi.org/10.5194/amt-12-1935-2019)
1071 [1935-2019](https://doi.org/10.5194/amt-12-1935-2019), 2019.
1072
1073 Feng, L., Smith, S. J., Braun, C., Crippa, M., Gidden, M. J., Hoesly, R., Klimont, Z., van Marle,
1074 M., van den Berg, M., and van der Werf, G. R.: The generation of gridded emissions data for
1075 CMIP6, *Geosci. Model Dev.*, 13, 461–482, <https://doi.org/10.5194/gmd-13-461-2020>, 2020.
1076
1077 [Fisher, J. A., Murray, L. T., Jones, D. B. A., and Deutscher, N. M.: Improved method for linear](#)
1078 [carbon monoxide simulation and source attribution in atmospheric chemistry models](#)
1079 [illustrated using GEOS-Chem v9, *Geosci. Model Dev.*, 10, 4129–4144,](#)
1080 <https://doi.org/10.5194/gmd-10-4129-2017>, 2017.
1081
1082 Fountoukis, C. and Nenes, A.: Continued development of a cloud droplet formation
1083 parameterization for global climate models, *J. Geophys. Res. Atmos.*, 110, D11212,
1084 <https://doi.org/10.1029/2004JD005591>, 2005.
1085

Deleted:

1087 [Fricko O., Havlik P., Rogelj J., Klimont Z., Gusti M., Johnson N., Kolp P., Strubegger M., Valin](#)
1088 [H., Amann M., Ermolieva, T., Forsell, N., Herrero, M., Heyes, C., Kindermann, G.,](#)
1089 [Volker Krey, V., McCollum, D. L., Obersteiner, M., Shonali Pachauri, S., Shilpa Rao, S., Riahi,](#)
1090 [K., The marker quantification of the Shared Socioeconomic Pathway 2: a middle-of-the-road](#)
1091 [scenario for the 21st century. *Glob. Environ. Change*, 42, 251–267, 2017.](#)

1092

1093 [Froyd, K. D., Yu, P., Schill, G. P., Brock, C. A., Kupc, A., Williamson, C. J., Jensen, E. J. Ray,](#)
1094 [E., Rosenlof, K. H., Bian, H., Darmenov, A. S., Colarco, P. R., Diskin, G. S., Bui, T. P., and](#)
1095 [Murphy, D. M., Global-scale measurements reveal cirrus clouds are seeded by mineral dust](#)
1096 [aerosol, *Nat. Geosci.*, Volume 15, Issue 3, p.177-183, 10.1038/s41561-022-00901-w, Feb, 2022.](#)

1097

1098 [Fung K. M., Heald, C.L., Kroll, J.H., Wang, S., Jo, D.S., Gettelman, A., Lu, Z., Liu, X.,](#)
1099 [Zaveri, R. A., Apel, E. C., Blake, D., R., Jimenez, J., Campuzano-Jost, P., Veres, P. R., Bates, T.](#)
1100 [S., Shilling, J. E., and Zawadowicz, M., Exploring dimethyl sulfide \(DMS\) oxidation and](#)
1101 [implications for global aerosol radiative forcing. *Atmos. Chem. and Phys.*, 22, 2:1549-1573,](#)
1102 [PNNL-SA-166358, \[https://doi:10.5194/acp-22-1549-2022\]\(https://doi.org/10.5194/acp-22-1549-2022\), 2022.](#)

1103

1104 Galí, M., Levasseur, M., Devred, E., Simó, R., and Babin, M.: Sea-surface dimethylsulfide
1105 (DMS) concentration from satellite data at global and regional scales, *Biogeosciences*, 15, 3497–
1106 3519, <https://doi.org/10.5194/bg-15-3497-2018>, 2018.

1107

1108 [Gao, C. Y., Heald, C. L., Katich, J. M., Luo, G., Yu, F., Remote Aerosol Simulated During the](#)
1109 [Atmospheric Tomography \(ATom\) Campaign and Implications for Aerosol Lifetime. *J.*](#)
1110 [Geophys. Res. Atmos., Vol. 127, I. 22, <https://doi.org/10.1029/2022JD036524>, 2022.](#)

1111

1112 Gliš, J., Mortier, A., Schulz, M., Andrews, E., Balkanski, Y., Bauer, S. E., Benedictow, A. M.
1113 K., Bian, H., Checa-Garcia, R., Chin, M., Ginoux, P., Griesfeller, J. J., Heckel, A., Kipling, Z.,
1114 Kirkevåg, A., Kokkola, H., Laj, P., Le Sager, P., Lund, M. T., Lund Myhre, C., Matsui, H.,
1115 Myhre, G., Neubauer, D., van Noije, T., North, P., Olivie, D. J. L., Rémy, S., Sogacheva, L.,
1116 Takemura, T., Tsigaridis, K., and Tsyro, S. G.: AeroCom phase III multi-model evaluation of the
1117 aerosol life cycle and optical properties using ground- and space-based remote sensing as well as
1118 surface in situ observations, *Atmos. Chem. Phys.*, 21, 87–128, <https://doi.org/10.5194/acp-21-87->
1119 2021, Jan., 2021.

1120

1121 Grennfelt, P., Engleryd, A., Forsius, M., Hov, Ø., Rodhe, H., and Cowling, E.: Acid rain and air
1122 pollution: 50 years of progress in environmental science and policy, *Ambio*, 49, 849–864,
1123 <https://doi.org/10.1007/s13280-019-01244-4>, 2020.

1124

1125 Gryspeerdt, E., Povey, A. C., Grainger, R. G., Hasekamp, O., Hsu, N. C., Mulcahy, J. P., Sayer,
1126 A. M., and Sorooshian, A.: Uncertainty in aerosol-cloud radiative forcing is driven by clean
1127 conditions, *Atmos. Chem. Phys.*, 23, 4115–4122, <https://doi.org/10.5194/acp-23-4115-2023>,
1128 2023.

1129

1130 Guo, H., Campuzano-Jost, P., Nault, B. A., Day, D. A., Schroder, J. C., Kim, D., Dibb, J. E.,
1131 Dollner, M., Weinzierl, B., and Jimenez, J. L.: The importance of size ranges in aerosol

1132 instrument intercomparisons: a case study for the Atmospheric Tomography Mission, *Atmos.*
1133 *Meas. Tech.*, 14, 3631–3655, 2021.

1134

1135 Hodshire, A. L., Campuzano-Jost, P., Kodros, J. K., Croft, B., Nault, B. A., Schroder, J. C.,
1136 Jimenez, J. L., and Pierce, J. R.: The potential role of methanesulfonic acid (MSA) in aerosol
1137 formation and growth and the associated radiative forcings, *Atmos. Chem. Phys.*, 19, 3137–
1138 3160, 2019.

1139

1140 Hodzic, A., Campuzano-Jost, P., Bian, H., Chin, M., Colarco, P. R., Day, D. A., Froyd, K. D.,
1141 Heinold, B., Jo, D. S., Katich, J. M., Kodros, J. K., Nault, B. A., Pierce, J. R., Ray, E., Schacht,
1142 J., Schill, G. P., Schroder, J. C., Schwarz, J. P., Sueper, D. T., Tegen, I., Tilmes, S., Tsigaridis,
1143 K., Yu, P., and Jimenez, J. L.: Characterization of organic aerosol across the global remote
1144 troposphere: a comparison of ATom measurements and global chemistry models, *Atmos. Chem.*
1145 *Phys.*, 20, 4607–4635, 2020.

1146

1147 Hoffmann, E. H., Tilgner, A., Schrödner, R., Bräuer, P., Wolke, R. and Herrmann, H., An
1148 advanced modeling study on the impacts and atmospheric implications of multiphase dimethyl
1149 sulfide chemistry, *Proc. Natl. Acad. Sci. USA*, 113, 11776–11781,
1150 <https://doi.org/10.1073/pnas.1606320113>, 2016.

1151

1152 Holton, J. R., Haynes, P. H., McIntyre, M. E., Douglass, A. R., Rood, R. B., and Pfister, L.:
1153 Stratosphere-troposphere exchange, *Rev. Geophys.*, 33, 403–439,
1154 <https://doi.org/10.1029/95RG02097>, 1995.

1155

1156 Hoesly, R. M., Smith, S. J., Feng, L., Klimont, Z., Janssens-Maenhout, G., Pitkanen, T., et al.
1157 (2018). Historical (1750–2014) anthropogenic emissions of reactive gases and aerosols from the
1158 Community Emissions Data System (CEDS). *Geosci. Model Dev.*, 11,
1159 369–408. <https://doi.org/10.5194/gmd-11-369-2018>.

1160

1161 Huang, R.-J., Duan, J., Li, Y., Chen, Q., Chen, Y., Tang, M., Yang, L., Ni, H., Lin, C., Xu, W.,
1162 Liu, Y., Chen, C., Yan, Z., Ovadnevaite, J., Ceburnis, D., Dusek, U., Cao, J., Hoffmann, T., &
1163 O'Dowd, C. D., Effects of NH₃ and alkaline metals on the formation of particulate sulfate and
1164 nitrate in wintertime Beijing. *Sci. Total Environ.*, 717, 137190,
1165 <https://doi.org/10.1016/j.scitotenv.2020.137190>, 2020.

1166

1167 Huey, L. G., Tanner, D. J., Slusher, D. L., Dibb, J. E., Arimoto, R., Chen, G., Davis, D., Buhr,
1168 M. P., Nowak, J. B., Mauldin III, R. L., Eisele, F. L., and Kosciuch, E.: CIMS measurements of
1169 HNO₃ and SO₂ at the South Pole during ISCAT 2000, *Atmos. Environ.*, 38, 5411–5421,
1170 <https://doi.org/10.1016/j.atmosenv.2004.04.037>, 2004.

1171

1172 [Ikeda, K., Tanimoto, H., Sugita, T., Akiyoshi, H., Kanaya, Y., Zhu, C., and Taketani, F.: Tagged](#)
1173 [tracer simulations of black carbon in the Arctic: transport, source contributions, and budget,](#)
1174 [Atmos. Chem. Phys., 17, 10515–10533, <https://doi.org/10.5194/acp-17-10515-2017>, 2017.](#)

1175

1176 Jia, H., Ma, X., Yu, F., and Quaas, J.: Significant underestimation of radiative forcing by
1177 aerosol–cloud interactions derived from satellite-based methods, *Nat. Commun.*, 12,
1178 <https://doi.org/10.1038/s41467-021-23888-1>, 2021.

1179
1180 Jia, H., Quaas, J., Gryspeerdt, E., Böhm, C., and Sourdeval, O.: Addressing the difficulties in
1181 quantifying the Twomey effect for marine warm clouds from multi-sensor satellite observations
1182 and reanalysis, *Atmos. Chem. Phys.*, 22, 7353–7372, <https://doi.org/10.5194/acp-22-7353-2022>,
1183 2022.

1184
1185 [Lin, X., Keppel-Aleks, G., Rogers, B. M., Birch, L.: Simulated CO2 tracer concentrations in the](https://doi.org/10.7302/rp59-rw53)
1186 [Northern Hemisphere from a tagged transport model GEOS-Chem v12.0.0 \[Data set\], University](https://doi.org/10.7302/rp59-rw53)
1187 [of Michigan - Deep Blue Data. <https://doi.org/10.7302/rp59-rw53>, 2020.](https://doi.org/10.7302/rp59-rw53)

1188
1189 Moch, J. M., Mickley, L. J., Keller, C. A., Bian, H., Lundgren, E. W., Zhai, S., and Jacob, D. J.:
1190 Aerosol-radiation interactions in China in winter: Competing effects of reduced shortwave
1191 radiation and cloud-snowfall-albedo feedbacks under rapidly changing emissions, *J. Geophys.*
1192 *Res. Atmos.*, 127, e2021JD035442, <https://doi.org/10.1029/2021JD035442>, 2022.

1193 [Myhre, G., B. H., Samset, M. Schulz, Y. Balkanski, S. Bauer, T. K. Berntsen, H. Bian, N.](https://doi.org/10.5194/acp-13-1853-2013)
1194 [Bellouin, M. Chin, T. Diehl, R. C. Easter, J. Feichter, S. J. Ghan, D. Hauglustaine, T. Iversen, S.](https://doi.org/10.5194/acp-13-1853-2013)
1195 [Kinne, A. Kirkevåg, J.-F. Lamarque, G. Lin, X. Liu, G. Luo, X. Ma, J. E. Penner, P. J. Rasch, Ø.](https://doi.org/10.5194/acp-13-1853-2013)
1196 [Seland, R. B. Skeie, P. Stier, T. Takemura, K. Tsigaridis, Z. Wang, L. Xu, H. Yu, F. Yu, J.-H.](https://doi.org/10.5194/acp-13-1853-2013)
1197 [Yoon, K. Zhang, H. Zhang, and C. Zhou, Radiative forcing of the direct aerosol effect from](https://doi.org/10.5194/acp-13-1853-2013)
1198 [AeroCom Phase II simulations, *Atmos. Chem. Phys.*, 13, 1853-1877, doi:10.5194/acp-13-1853-](https://doi.org/10.5194/acp-13-1853-2013)
1199 [2013, 2013.](https://doi.org/10.5194/acp-13-1853-2013)

1200
1201 Josephson, D. C., Robinson, J. M., Chiotti, J., Jirka, K. J., and Kraft, C. E.: Chemical and
1202 biological recovery from acid deposition within the Honnedaga Lake watershed, New York,
1203 USA, *Environ. Monit. Assess.*, 186, 4391–4409, <https://doi.org/10.1007/s10661-014-3706-9>,
1204 2014.

1205
1206 Jurkat, T., Kaufmann, S., Voigt, C., Schäuble, D., Jeßberger, P., and Ziereis, H.: The airborne
1207 mass spectrometer AIMS – Part 2: Measurements of trace gases with stratospheric or tropo-
1208 spheric origin in the UTLS, *Atmos. Meas. Tech.*, 9, 1907–1923, [https://doi.org/10.5194/amt-9-](https://doi.org/10.5194/amt-9-1907-2016)
1209 [1907-2016](https://doi.org/10.5194/amt-9-1907-2016), 2016.

1210
1211 [Katich, J. M., Samset, B. H., Paul Bui, T., Dollner, M., Froyd, K. D., Campuzano-Jost, P.,](https://doi.org/10.1029/2018JD029206)
1212 [Nault, B. A., Schroder, J. C., Weinzierl, B., Schwarz J. P., Strong Contrast in Remote Black](https://doi.org/10.1029/2018JD029206)
1213 [Carbon Aerosol Loadings Between the Atlantic and Pacific Basins, *Journal of Geophysical*](https://doi.org/10.1029/2018JD029206)
1214 [Research: Atmospheres, Volume 123, Issue 23 p. 13,386-13,395,](https://doi.org/10.1029/2018JD029206)
1215 <https://doi.org/10.1029/2018JD029206>, 2018.

1216
1217 Kettle, A. J. and Andreae, M. O.: Flux of dimethylsulfide from the oceans: A comparison of
1218 updated data sets and flux models, *J. Geophys. Res. Atmos.*, 105, 26793–26808,
1219 <https://doi.org/10.1029/2000JD900252>, 2000.

1220
1221 Klein, S. A., Zhang, Y., Zelinka, M. D., Pincus, R., Boyle, J., and Gleckler, P. J.: Are climate
1222 model simulations of clouds improving? An evaluation using the ISCCP simulator, *J. Geophys.*
1223 *Res. Atmos.*, 118, 1329–1342, <https://doi.org/10.1002/jgrd.50141>, 2013.

1224

1225 Lana, A., Bell, T. G., Simó, R., Vallina, S. M., Ballabrera-Poy, J., Kettle, A. J., Dachs, J., Bopp,
1226 L., Saltzman, E. S., Stefels, J., Johnson, J. E., and Liss, P. S.: An updated climatology of surface
1227 dimethylsulfide concentrations and emission fluxes in the global ocean, *Global Biogeochem.*
1228 *Cy.*, 25, GB1004, doi:10.1029/2010GB003850, 2011.

1229
1230 [Liss, P.S., and Merlivat, L., Air-sea gas exchange rates: Introduction and synthesis, in *The Role*
1231 *of Air-Sea Gas Exchange in Geochemical Cycling*, edited by P. Buat-Menard, pp. 113-127, D.
1232 *Reidel, Norwell, Mass., 1986.*](#)

1233
1234 Liu, M. and Matsui, H.: Improved simulations of global black carbon distributions by modifying
1235 wet scavenging processes in convective and mixed-phase clouds, *J. Geophys. Res. Atmos.*, 126,
1236 e2020JD033890, <https://doi.org/10.1029/2020JD033890>, 2021.

1237
1238 Lund, M. T., Myhre, G., Haslerud, A. S., Skeie, R. B., Griesfeller, J., Platt, S. M., Kumar, R.,
1239 Myhre, C. L., and Schulz, M.: Concentrations and radiative forcing of anthropogenic aerosols
1240 from 1750 to 2014 simulated with the Oslo CTM3 and CEDS emission inventory, *Geosci. Model*
1241 *Dev.*, 11, 4909–4931, <https://doi.org/10.5194/gmd-11-4909-2018>, 2018.

1242
1243 Malavelle, F. F., Haywood, J. M., Jones, A., Gettelman, A., Clarisse, L., Bauduin, S., Allan, R.
1244 P., Karset, I. H. H., Kristjánsson, J. E., Oreopoulos, L., Cho, N., Lee, D., Bellouin, N., Boucher,
1245 O., Grosvenor, D. P., Carslaw, K. S., Dhomse, S., Mann, G. W., Schmidt, A., Coe, H., Hartley,
1246 M. E., Dalvi, M., Hill, A. A., Johnson, B. T., Johnson, C. E., Knight, J. R., O'Connor, F. M.,
1247 Partridge, D. G., Stier, P., Myhre, G., Platnick, S., Stephens, G. L., Takahashi, H., and
1248 Thordarson, T.: Strong constraints on aerosol–cloud interactions from volcanic eruptions,
1249 *Nature*, 546, 485–491, <https://doi.org/10.1038/nature22974>, 2017.

1250
1251 McDonnell, T. C., Driscoll, C. T., Sullivan, T. J., Burns, D. A., Baldigo, B. P., Shao, S., and
1252 Lawrence, G. B.: Regional target loads of atmospheric nitrogen and sulfur deposition for the
1253 protection of stream and watershed soil resources of the Adirondack Mountains, USA, *Environ.*
1254 *Pollut.*, 281, 117110, <https://doi.org/10.1016/j.envpol.2021.117110>, 2021.

1255
1256 Matsui, H.: Development of a global aerosol model using a two-dimensional sectional method: 1.
1257 Model design, *J. Adv. Model. Earth Syst.*, 9, 1921–1947,
1258 <https://doi.org/10.1002/2017MS000936>, 2017.

1259
1260 Matsui, H. and Mahowald, N.: Development of a global aerosol model using a two-dimensional
1261 sectional method: 2. Evaluation and sensitivity simulations, *J. Adv. Model. Earth Syst.*, 9, 1887–
1262 1920, <https://doi.org/10.1002/2017MS000937>, 2017.

1263
1264 Molod, A.: Constraints on the Total Water PDF in GCMs from AIRS and a High Resolution
1265 Model, *J. Climate*, 25, 8341–8352, <https://doi.org/10.1175/JCLI-D-11-00412.1>, 2012.

1266
1267 Moorthi, S. and Suarez, M. J.: Relaxed Arakawa-Schubert. A parameterization of moist
1268 convection for general circulation models, *Mon. Weather Rev.*, 120, 978–1002,
1269 [https://doi.org/10.1175/1520-0493\(1992\)120<0978:RASAPO>2.0.CO;2](https://doi.org/10.1175/1520-0493(1992)120<0978:RASAPO>2.0.CO;2), 1992.

1270

1271 Myhre, G., Samset, B. H., Schulz, M., Balkanski, Y., Bauer, S., Bernsten, T. K., Bian, H.,
1272 Bellouin, N., Chin, M., Diehl, T., Easter, R. C., Feichter, J., Ghan, S. J., Hauglustaine, D.,
1273 Iversen, T., Kinne, S., Kirkevåg, A., Lamarque, J.-F., Lin, G., Liu, X., Lund, M. T., Luo, G., Ma,
1274 X., van Noije, T., Penner, J. E., Rasch, P. J., Ruiz, A., Seland, Ø., Skeie, R. B., Stier, P.,
1275 Takemura, T., Tsigaridis, K., Wang, P., Wang, Z., Xu, L., Yu, H., Yu, F., Yoon, J.-H., Zhang,
1276 K., Zhang, H., and Zhou, C.: Radiative forcing of the direct aerosol effect from AeroCom Phase
1277 II simulations, *Atmos. Chem. Phys.*, 13, 1853–1877, <https://doi.org/10.5194/acp-13-1853-2013>,
1278 2013.

1279 [Nicely, J. M., Duncan, B. N., Hancox, T. F., Wolfe, G. M., Salawitch, R. J., Deushi, M.,
1280 Haslerud, A. S., Jöckel, P., Josse, B., Kinnison, D. E., Klekociuk, A., Manyin, M. E., Marécal,
1281 V., Morgenstern, O., Murray, L. T., Myhre, G., Oman, L. D., Pitari, G., Pozzer, A., Quaglia, L.,
1282 Revell, L. E., Rozanov, E., Stenke, A., Stone, K., Strahan, S., Tilmes, S., Tost, H., Westervelt, D.,
1283 M., and Zeng, G.: A machine learning examination of hydroxyl radical differences among model
1284 simulations for CCMI-1, *Atmos. Chem. Phys.*, 20, 1341–1361, \[https://doi.org/10.5194/acp-20-
1285 1341-2020\]\(https://doi.org/10.5194/acp-20-1341-2020\), 2020.](#)

1287 [Nielsen, J. E., Pawson, S., Molod, A., Auer, B., da Silva, A. M., Douglass, A. R., Wargan, K.:
1288 Chemical mechanisms and their applications in the Goddard Earth Observing System
1289 \(GEOS\) earth system model. *J. Adv. Model. Earth Sys.*, 9, 3019–3044.
1290 <https://doi.org/10.1002/2017MS001011>, 2017.](#)

1292
1293 Nightingale P. D., Malin G., Law C. S., Watson A. J., Liss P. S., Liddicoat M. I., et al. In
1294 situ evaluation of air-sea gas exchange parameterizations using novel conservative and volatile
1295 tracers. *Global Biogeochem. Cy.* 14, 373–387, <https://doi.org/10.1029/1999gb900091>, 2000.

1296
1297 Penner, A., Prather, J. E., Ramanathan, K. A., Ramaswamy, V., Rasch, V., Ravishankara, P. J.,
1298 Rosenfeld, A. R., Stephens, D., and Wood, R.: Improving our fundamental understanding of the
1299 role of aerosol–cloud interactions in the climate system, *P. Natl. Acad. Sci. USA*, 113, 5781–
1300 5790, <https://doi.org/10.1073/pnas.1514043113>, 2016.

1301
1302 Rasch, P. J., Xie, S., Ma, P. -L., Lin, W., Wang, H., Tang, Q., Burrows, S. M., Caldwell, P.,
1303 Zhang, K., Easter, R. C., Cameron-Smith, P., Singh, B., Wan, H., Golaz, J.-C., Harrop, B. E.,
1304 Roesler, E., Bacmeister, J., Larson, V. E., Evans, K. J., Qian, Y., Taylor, M., Leung, L. R.,
1305 Zhang, Y., Brent, L., Branstetter, M., Hannay, C., Mahajan, S., Mامتjanov, A., Neale, R.,
1306 Richter, J. H., Yoon, J.-H., Zender, C. S., Bader, D., Flanner, M., Foucar, J. G., Jacob, R., Keen,
1307 N., Klein, S. A., Liu, X., Salinger, A. G., Shrivastava, M., and Yang, Y.: An Overview of the
1308 Atmospheric Component of the Energy Exascale Earth System Model, *J. Adv. Model. Earth
1309 Syst.*, 11, 2377–2411, <https://doi.org/10.1029/2019MS001629>, 2019.

1310
1311 Rickly, P. S., Xu, L., Crouse, J. D., Wennberg, P. O., and Rollins, A. W.: Improvements to a
1312 laser-induced fluorescence instrument for measuring SO₂ – impact on accuracy and precision,
1313 *Atmos. Meas. Tech.*, 14, 2429–2439, <https://doi.org/10.5194/amt-14-2429-2021>, 2021.

1314
1315 Rienecker, M., Suarez, M., Todling, R., Bacmeister, J., Takacs, L., Liu, H.-C., Gu, W.,
1316 Sienkiewicz, M., Koster, R., Gelaro, R., Stajner, I., and Nielsen, J.: The GEOS-5 Data

1317 Assimilation System – Documentation of Versions 5.0.1, 5.1.0, and 5.2.0., Vol. 27 of Technical
1318 Report Series on Global Modeling and Data Assimilation, NASA Goddard Space Flight Center,
1319 Greenbelt, MD, USA, 2008.
1320
1321 Rissman, T. A., Nenes, A., and Seinfeld, J. H.: Chemical amplification (or dampening) of the
1322 Twomey effect: Conditions derived from droplet activation theory, *J. Atmos. Sci.*, 61(8), 919–
1323 930, [https://doi.org/10.1175/1520-0469\(2004\)061<0919:CAODOT>2.0.CO;2](https://doi.org/10.1175/1520-0469(2004)061<0919:CAODOT>2.0.CO;2), 2004.
1324
1325 Rollins, A. W., Thornberry, T. D., Ciciora, S. J., McLaughlin, R. J., Watts, L. A., Hanisco, T. F.,
1326 Baumann, E., Giorgetta, F. R., Bui, T. V., Fahey, D. W., and Gao, R.-S.: A laser-induced
1327 fluorescence instrument for aircraft measurements of sulfur dioxide in the upper troposphere and
1328 lower stratosphere, *Atmos. Meas. Tech.*, 9, 4601–4613, [https://doi.org/10.5194/amt-9-4601-](https://doi.org/10.5194/amt-9-4601-2016)
1329 2016, 2016.
1330
1331 [Saltzman, E. S., King, D. B., Holmen, K., and Leck, C., Experimental Determination of the](#)
1332 [Diffusion Coefficient of Dimethylsulfide in Water, *J. of Geophys. Res. Atmos.*, Vol. 98, No. C9,](#)
1333 [16,481-16,486, 1993.](#)
1334
1335 [Schill, G. P., Froyd, K. D., Bian, H., Kupc, A., Williamson, C., Brock, C. B., Ray, E.,](#)
1336 [Hornbrook, R. S., Hills, A. J., Apel, E. C., Chen, M., Colarco, P., and Murphy, D. M., The](#)
1337 [ubiquity of dilute, aged smoke in the global remote troposphere and its effect on climate. *Nature*](#)
1338 [Geoscience](#), 13(6), <https://doi:10.1038/s41561-020-0586-1>, Jun., 2020.
1339
1340 Schueneman, M. K., Nault, B. A., Campuzano-Jost, P., Jo, D. S., Day, D. A., Schroder, J. C.,
1341 Palm, B. B., Hodzic, A., Dibb, J. E., and Jimenez, J. L.: Aerosol pH indicator and organosulfate
1342 detectability from aerosol mass spectrometry measurements, *Atmos. Meas. Tech.*, 14, 2237–
1343 2260, 2021.
1344
1345 Seinfeld, J. H., Bretherton, C., Carslaw, K. S., Coe, H., DeMott, P. J., Dunlea, E. J., Feingold, G.,
1346 Ghan, S., Guenther, A. B., Kahn, R., Kraucunas, I., Kreidenweis, S. M., Molina, M. J., Nenes,
1347 A., Penner, J. E., Prather, K. A., Ramanathan, V., Ramaswamy, V., Rasch, P. J., Ravishankara,
1348 A. R., Rosenfeld, D., Stephens, G., and Wood, R.: Improving our fundamental understanding of
1349 the role of aerosol–cloud interactions in the climate system, *P. Natl. Acad. Sci. USA*, 113, 5781–
1350 5790, <https://doi.org/10.1073/pnas.151404311>, 2016.
1351
1352 Schulz, M., Textor, C., Kinne, S., Balkanski, Y., Bauer, S., Berntsen, T., Berglen, T., Boucher,
1353 O., Dentener, F., Guibert, S., Isaksen, I. S. A., Iversen, T., Koch, D., Kirkevåg, A., Liu, X.,
1354 Montanaro, V., Myhre, G., Penner, J. E., Pitari, G., Reddy, S., Seland, Ø., Stier, P., and
1355 Takemura, T.: Radiative forcing by aerosols as derived from the AeroCom present-day and pre-
1356 industrial simulations, *Atmos. Chem. Phys.*, 6, 5225–5246, [https://doi.org/10.5194/acp-6-5225-](https://doi.org/10.5194/acp-6-5225-2006)
1357 2006, 2006
1358
1359 Simpson, I. J., Colman, J. J., Swanson, A. L., Bandy, A. R., Thornton, D. C., Blake, D. R., and F.
1360 S. Rowland, F. S.: Aircraft Measurements of Dimethyl Sulfide (DMS) Using a Whole Air
1361 Sampling Technique, *J. Atmos. Chem.*, 39, 191-213, <https://doi.org/10.1023/A:1010608529779>,
1362 2001.

Deleted:

1364
1365 Slingo, J.: The development and verification of a cloud prediction scheme for the ECMWF
1366 model, *Q. J. Roy. Meteor. Soc.*, 113, 899–927, <https://doi.org/10.1002/qj.49711347710>, 1987.
1367
1368 Smith, R. N. B.: A scheme for predicting layer clouds and their water content in a general
1369 circulation model, *Q. J. Roy. Meteor. Soc.*, 116, 435–460,
1370 <https://doi.org/10.1002/qj.49711649210>, 1990.
1371
1372 Søvde, O. A., Prather, M. J., Isaksen, I. S. A., Berntsen, T. K., Stordal, F., Zhu, X., Holmes, C.
1373 D., and Hsu, J.: The chemical transport model Oslo CTM3, *Geosci. Model Dev.*, 5, 1441–1469,
1374 <https://doi.org/10.5194/gmd-5-1441-2012>, 2012.
1375
1376 [Strode, S. A., Liu, J., Lait, L., Commane, R., Daube, B., Wofsy, S., Conaty, A., Newman, P., and](#)
1377 [Prather, M.: Forecasting carbon monoxide on a global scale for the ATom-1 aircraft mission:](#)
1378 [insights from airborne and satellite observations and modeling, *Atmos. Chem. Phys.*, 18, 10955–](#)
1379 [10971, <https://doi.org/10.5194/acp-18-10955-2018>, 2018.](#)
1380
1381 Tan, J., Fu, J. S., Dentener, F., Sun, J., Emmons, L., Tilmes, S., Flemming, J., Takemura, T.,
1382 Bian, H., Zhu, Q., Yang, C.-E., and Keating, T.: Source contributions to sulfur and nitrogen
1383 deposition – an HTAP II multi-model study on hemispheric transport, *Atmos. Chem. Phys.*, 18,
1384 12223–12240, <https://doi.org/10.5194/acp-18-12223-2018>, 2018.
1385
1386 Thompson, C. R., Wofsy, S. C., Prather, M. J., Newman, P. A., Hanisco, T. F., Ryerson, T. B.,
1387 Fahey, D. W., Apel, E. C., Brock, C. A., Brune, W. H., Froyd, K., Katich, J. M., Nicely, J. M.,
1388 Peischl, J., Ray, E., Veres, P. R., Wang, S., Allen, H. M., Asher, E., Bian, H., Blake, D.,
1389 Bourgeois, I., Budney, J., Paul Bui, T., Butler, A., Campuzano-Jost, P., Chang, C., Chin, M.,
1390 Commane, R., Correa, G., Crouse, J. D., Daube, B., Dibb, J. E., Digangi, J. P., Diskin, G. S.,
1391 Dollner, M., Elkins, J. W., Fiore, A. M., Flynn, C. M., Guo, H., Hall, S. R., Hannun, R. A., Hills,
1392 A., Hints, E. J., Hodzic, A., Hornbrook, R. S., Greg Huey, L., Jimenez, J. L., Keeling, R. F.,
1393 Kim, M. J., Kupc, A., Lacey, F., Lait, L. R., Lamarque, J.-F., Liu, J., Mckain, K., Meinardi, S.,
1394 Miller, D. O., Montzka, S. A., Moore, F. L., Morgan, E. J., Murphy, D. M., Murray, L. T., Nault,
1395 B. A., Andrew Neuman, J., Nguyen, L., Gonzalez, Y., Rollins, A., Rosenlof, K., Sargent, M.,
1396 Schill, G., Schwarz, J. P., St. Clair, J. M., Steenrod, S. D., Stephens, B. B., Strahan, S. E., Strode,
1397 S. A., Sweeney, C., Thames, A. B., Ullmann, K., Wagner, N., Weber, R., Weinzierl, B.,
1398 Wennberg, P. O., Williamson, C. J., Wolfe, G. M., and Zeng, L.: THE NASA ATMOSPHERIC
1399 TOMOGRAPHY (ATom) MISSION: Imaging the Chemistry of the Global Atmosphere, *Bull.*
1400 *Am. Meteorol. Soc.*, 103, E761-E790, <https://doi.org/10.1175/BAMS-D-20-0315.1>, 2022.
1401
1402 Tiedtke, M.: Representation of clouds in large-scale models, *Mon. Weather Rev.*, 121, 3040–
1403 3061, [https://doi.org/10.1175/1520-0493\(1993\)121<3040:ROCILS>2.0.CO;2](https://doi.org/10.1175/1520-0493(1993)121<3040:ROCILS>2.0.CO;2), 1993.
1404
1405 Wang, H., Easter, R. C., Zhang, R., Ma, P., Singh, B., Zhang, K., Ganguly, D., Rasch, P. J.,
1406 Burrows, S. M., Ghan, S. J., Lou, S., Qian, Y., Yang, Y., Feng, Y., Flanner, M., Leung, L. R.,
1407 Liu, X., Shrivastava, M., Sun, J., Tang, Q., Xie, S., and Yoon, J.: Aerosols in the E3SM Version
1408 1: New Developments and Their Impacts on Radiative Forcing, *J. Adv. Model. Earth Syst.*, 12,
1409 e2019MS001851, <https://doi.org/10.1029/2019MS001851>, 2020.
1410
1411

1411 Wang, D., Zhu, B., Wang, H., and Sun, L., Simulation study on the indirect effect of sulfate on
1412 the summer climate over the eastern China monsoon region, *Sci. Rep.*, 11, 8295,
1413 <https://doi.org/10.1038/s41598-021-87832-5>, 2021.
1414
1415 Williamson, C. J., Kupc, A., Axisa, D., Bilsback, K. R., Bui, T. P., Campuzano-Jost, P., Dollner,
1416 M., Froyd, K. D., Hodshire, A. L., Jimenez, J. L., Kodros, J. K., Luo, G., Murphy, D. M., Nault,
1417 B. A., Ray, E. A., Weinzierl, B., Wilson, J. C., Yu, F., Yu, P., Pierce, J. R., and Brock, C. A.: A
1418 large source of cloud condensation nuclei from new particle formation in the tropics, *Nature*,
1419 574, 399–403, <https://doi.org/10.1038/s41586-019-1638-9>, 2019.
1420
1421 [Yan, J., Jung, J., Zhang, M., Xu, S., Lin, Q., Zhao, S., and Chen, L.: Significant Underestimation](#)
1422 [of Gaseous Methanesulfonic Acid \(MSA\) over Southern Ocean, *Environ. Sci. Technol.*, 53 \(22\),](#)
1423 [pp. 13064-13070, <https://doi.org/10.1021/acs.est.9b05362>, 2019.](#)
1424
1425 [Yu, P. F., Froyd, K. D., Portmann, R. W., Toon, O. B., Freitas, S. R., Bardeen, C. G., Brock, C.,](#)
1426 [Fan, T. Y., Gao, R. S., Katich, J. M., Kupc, A., Liu, S., Maloney, C., Murphy, D. M., Rosenlof,](#)
1427 [K. H., Schill, G., Schwarz, J. P., and Williamson, C.: Efficient In-Cloud Removal of Aerosols by](#)
1428 [Deep Convection, *Geophys. Res. Lett.*, 46, 1061–1069, <https://doi.org/10.1029/2018gl080544>,](#)
1429 [2019.](#)
1430
1431 Zhang, K., Zhang, W., Wan, H., Rasch, P. J., Ghan, S. J., Easter, R. C., Shi, X., Wang, Y.,
1432 Wang, H., Ma, P.-L., Zhang, S., Sun, J., Burrows, S. M., Shrivastava, M., Singh, B., Qian, Y.,
1433 Liu, X., Golaz, J.-C., Tang, Q., Zheng, X., Xie, S., Lin, W., Feng, Y., Wang, M., Yoon, J.-H.,
1434 and Leung, L. R.: Effective radiative forcing of anthropogenic aerosols in E3SM version 1:
1435 historical changes, causality, decomposition, and parameterization sensitivities, *Atmos. Chem.*
1436 *Phys.*, 22, 9129–9160, <https://doi.org/10.5194/acp-22-9129-2022>, 2022.
1437
1438 Zhu, J., Penner, J. E., Lin, G., Zhou, C., Xu, L., and Zhuang, B.: Mechanism of SOA formation
1439 determines magnitude of radiative effects. *Proceedings of the National Academy of Sciences of*
1440 *the United States of America*, 114, 12685–12690, [https://doi.org/10.1073/](https://doi.org/10.1073/pnas.1712273114)
1441 [pnas.1712273114](#), 2017.
1442
1443 Zhu, J., Penner, J. E., Yu, F., Sillman, S., Andreae, M. O., and Coe, H.: Decrease in radiative
1444 forcing by organic aerosol nucleation, climate, and land use change. *Nature Commun.*, 10, 423,
1445 <https://doi.org/10.1038/s41467-019-08407-7>, 2019.
1446
1447
1448
1449
1450
1451
1452
1453
1454
1455
1456
1457

1458 Table 1. ATom sulfur measurements used in the study

| Instrument | SO ₄ | | SO ₂ | | MSA | | DMS | |
|-----------------------------|---|---|---|----------------------|---------------------------------------|-------------------------------|-------------------|----------------------|
| | AMS ^a | PALMS ^b | CIMS ^c | LIF ^d | AMS | PALMS | TOGA ^e | WAS ^f |
| ATom deployment(s) | 1 to 4 | 1 to 4 | 1 to 4 | 4 | 1 to 4 | 1 to 4 | 2 to 4 | 1 to 4 |
| Frequency | 60 s | 180 s | 1 s | 1 s | 1 s | 180 s | 120 s | Variable but ~180 s |
| Accuracy | ±35% (2s) | ±60% at 10 ng m ⁻³ ±20% at 1 µg m ⁻³ | ±25% | ± 9% (1s) | ±35% (2s) | ±70% | 15% or better | 10% |
| Detection limit | 5-15 ng sm ⁻³ | ~10 ng sm ⁻³ | 130pptv | 2 pptv | 2.5 ng sm ⁻³ (60 s) | ~15 ng sm ⁻³ | 1 ppt | 1 ppt |
| Cut-off size (dry diameter) | ~0.75 µm | 0.1-3 µm | | | ~0.75 µm | 0.1-3 µm | | |
| Primary Investigator(s) | Jose Jimenez and Pedro Campuzano Jost | Karl Froyd and Gregory Schill | Paul Wennberg | Andrew Rollins | Jose Jimenez and Pedro Campuzano Jost | Karl Froyd and Gregory Schill | Eric Apel | Donald Blake |
| References | Guo et al., 2021; Schueneman et al., 2021 | Froyd et al., 2019 | Allen et al., 2022; Crouse et al., 2006 | Rollins et al., 2016 | Hodshire et al., 2019 | Froyd et al., 2019 | Apel et al., 2015 | Simpson et al., 2001 |

^aAMS: Aerosol Mass Spectrometer

^bPALMS: Particle Analysis by Laser Mass Spectrometry

^cCIMS: Chemical Ionization Mass Spectrometer

^dLIF: Laser Induced Fluorescence

^eTOGA: NCAR Trace Organic Gas Analyzer

^fWAS: Whole Air Sampler

1459
1460
1461
1462
1463
1464
1465
1466

Deleted:

Formatted: Superscript

Table 2. AeroCom Models used in this study

| Model Abbreviation | Model Version | Nominal Resolution | Vertical Levels | Meteorological Fields | Ocean Surface Temperature Data | Interactive Aerosol-Meteorology | Endogenous Oxidants | Endogenous DMS Emission | Aerosol Module | Anthropogenic Emission | Volcano Emission | Key References |
|--------------------|---------------|--------------------|-----------------|-----------------------|--------------------------------|---------------------------------|---------------------|-------------------------|--|---|---|---|
| CAM-ATRAS | CAM5-ATRAS2 | 1.9° × 2.5° | 30 | MERRA-2 | HadSST | Yes | Yes | No | Microphysics, 12 sectional size bins, and internal mixing of aerosol constituents in each bin. | CEDS (Hoesly et al., 2018) | Degassing (Andres and Kagnoc, 1998), Eruption (Neely and Schmidt, 2016) | Liu and Matsui 2021; Matsui 2017; Matsui and Mahowald, 2017 |
| E3SM | v1.0 | 1° × 1° | 72 | ERA-Interim | HadSST | Yes | No | No | Microphysics, MAM4, internal mixing within a mode, external mixing between modes | CEDS (Hoesly et al., 2018) | Continuous emission (Denener et al., 2006), No eruptive emissions. | Rasch et al., 2019; Wang et al., 2020; Zhang et al., 2022 |
| GEOS | Icarus-3 3 p2 | 1° × 1° | 72 | MERRA-2 | MERRA sst | Yes | No | Yes | GOCART, Bulk, external mixing | CEDS (Hoesly et al., 2018) | Carns et al., 2016, 2017 | Bian 2017; Colarco et al., 2010; Chin et al., 2000 |
| IMPACT | | 1.9° × 2.5° | 30 | Open IFS ECMWF | HadSST | No | Yes | no | Microphysics, internal mixing within a mode, external mixing between modes | CEDS (Hoesly et al., 2018) | AeroCom volcanic emissions | Zhu et al., 2017; Zhu et al., 2019 |
| OsloCTM3 | OsloCTM3v1.02 | 2.25° × 2.25° | 60 | Open IFS ECMWF | Open IFS ECMWF | No | Yes | Yes | Bulk, external mixing | SSP245 with linear interpolation for 2017 | AeroCom volcanic emissions, continuous from Dentener (2006) | Lund et al., 018; Svendsen et al. 2012 |

Deleted: (using TOMS- and OMI-based estimates),

Deleted: ¶

1467
1468

Table 3. DMS emission used/calculated by the five AeroCom models

| Model abbreviation | Emission inventory | DMS concentration in sea water | DMS flux calculation | Meteorological fields |
|--------------------|--------------------|--------------------------------|---|------------------------|
| CAM-ATRAS | No | Lana et al. (2011) | Nightingale et al. 2000 | Wind from ECMWF-IFS |
| E3SM | Yes | | | |
| GEOS | No | Lana et al. (2011) | Liss and Merlivat, (1986), Saltzman et al. (1993) | SST and wind from GEOS |
| IMPACT | Yes | | | |
| OsloCTM3 | No | Kettle and Andreae (2000) | Nightingale et al. (2000) | Wind from ECMWF-IFS |

Formatted: Danish

Formatted Table

1472
1473

Table 4. Global sulfur budget in 2017

| | | Emission | | SUPSO ₂ ¹ | SUPMSA | SUPSO ₄ | Dry | Wet | TotalSource | Burden | Lifetime |
|---------------|-----------------|----------|--------|---------------------------------|--------|--------------------|--------|--------|-------------|--------|----------|
| | | TgS/yr | TgS/yr | TgS/yr | TgS/yr | TgS/yr | TgS/yr | TgS/yr | TgS/yr | TgS | days |
| CAM- ATRAS | DMS | 26.05 | -26.05 | -- | -- | -- | -- | -- | 26.05 | 0.13 | 1.8 |
| | SO ₂ | 68.67 | 26.05 | -- | -55.67 | -39.05 | -- | -- | 94.72 | 0.445 | 1.7 |
| | SO ₄ | 1.76 | -- | -- | 55.67 | -4.72 | -53.23 | -- | 58.09 | 0.67 | 4.2 |
| E3SM | DMS | 19.43 | -19.40 | -- | -- | -- | -- | -- | 19.43 | 0.0658 | 1.24 |
| | SO ₂ | 67.92 | 19.40 | -- | -38.56 | -48.76 | -- | -- | 87.32 | 0.3825 | 1.60 |
| | SO ₄ | 1.74 | -- | -- | 38.56 | -6.95 | -33.31 | -- | 40.31 | 0.6183 | 5.60 |
| GEOS | DMS | 15.57 | -14.84 | -0.74 | -- | -- | -- | -- | 15.57 | 0.0252 | 0.59 |
| | SO ₂ | 67.06 | 14.84 | -- | -37.49 | -32.93 | -11.39 | -- | 81.90 | 0.3488 | 1.55 |
| | SO ₄ | 1.68 | -- | -- | 37.49 | -5.27 | -33.90 | -- | 39.17 | 0.3269 | 3.05 |
| | MSA | -- | -- | 0.74 | -- | -0.10 | -0.64 | -- | -0.74 | 0.0063 | 3.11 |
| IMPACT | DMS | 18.22 | -18.22 | -- | -- | -- | -- | -- | 18.05 | 0.0369 | 0.75 |
| | SO ₂ | 64.76 | 18.22 | -- | -51.44 | -31.29 | -- | -- | 82.98 | 0.4134 | 1.82 |
| | SO ₄ | 1.36 | -- | -- | 51.44 | -3.48 | -49.32 | -- | 52.80 | 0.7502 | 5.19 |
| OsloCTM3 | DMS | 26.93 | -26.93 | -- | -- | -- | -- | -- | 26.93 | 0.1496 | 2.03 |
| | SO ₂ | 52.80 | 26.93 | -- | -49.23 | -29.01 | -1.49 | -- | 79.73 | 0.2346 | 1.08 |
| | SO ₄ | 1.053 | -- | -- | 55.49 | -6.35 | -50.29 | -- | 56.54 | 0.8681 | 5.60 |

¹SUPSO₂: chemical production for SO₂

Deleted: 1

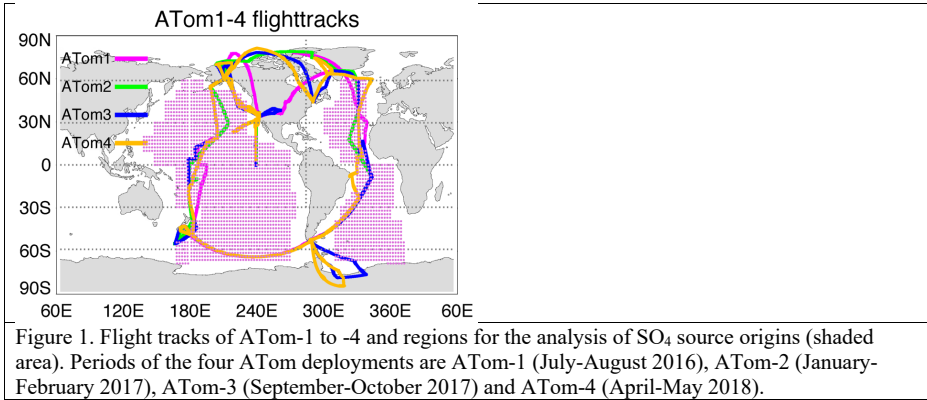
Deleted: 3

1474
1475
1476
1477

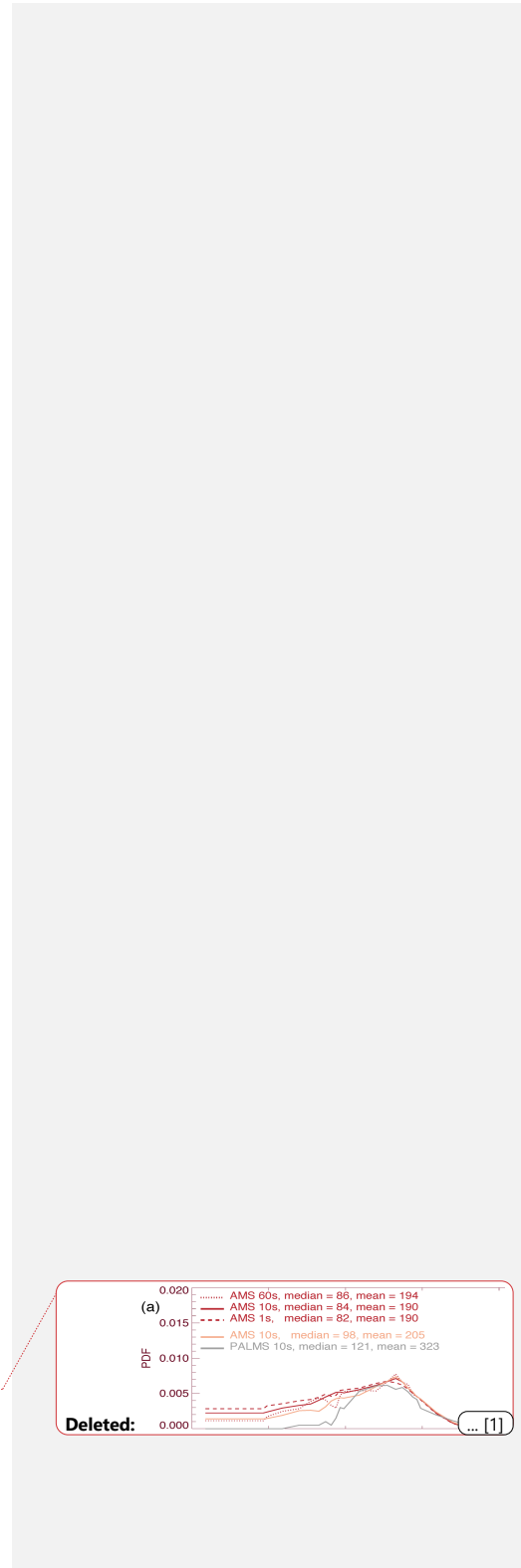
Table 5. Global and annual sulfate multimodel mean and diversity from three AeroCom phases

| reference | AeroCom-I | | AeroCom-II | | AeroCom-III | |
|-------------|---------------------|--------------------|----------------------|--|--|--|
| | Textor et al., 2006 | Myher et al., 2013 | Kipling et al., 2016 | Gliß et al., 2021 | This work | |
| Study year | 2000 | 2006 | 2006 | 2010 | 2017 | |
| # of models | 16 | 16 | 18 | 14 | 5 | |
| MMM (Tg) | 2.0 | 1.05 | 1.48 | 1.87 | 1.94 | |
| δ (%) | 25.0 | 26.4 | 34.6 | 38.8 | 28.0 | |
| observation | No | No | No | AC, AS, AE, and AOD from Ground station and AOD from MODIS | DMS, SO ₂ , SO ₄ and MSA from ATom | |

1478
1479
1480
1481
1482
1483
1484
1485
1486
1487
1488



1491
1492
1493
1494
1495
1496
1497
1498
1499
1500
1501
1502
1503
1504
1505
1506
1507
1508
1509
1510
1511
1512
1513
1514
1515
1516
1517
1518
1519
1520
1521
1522



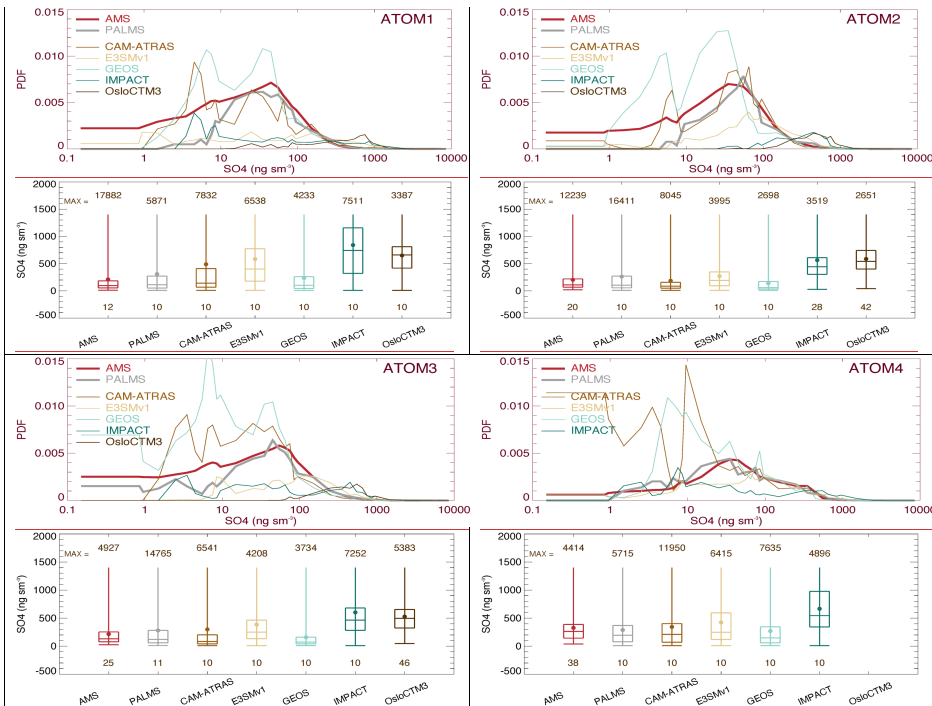
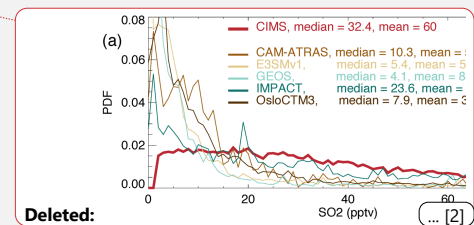
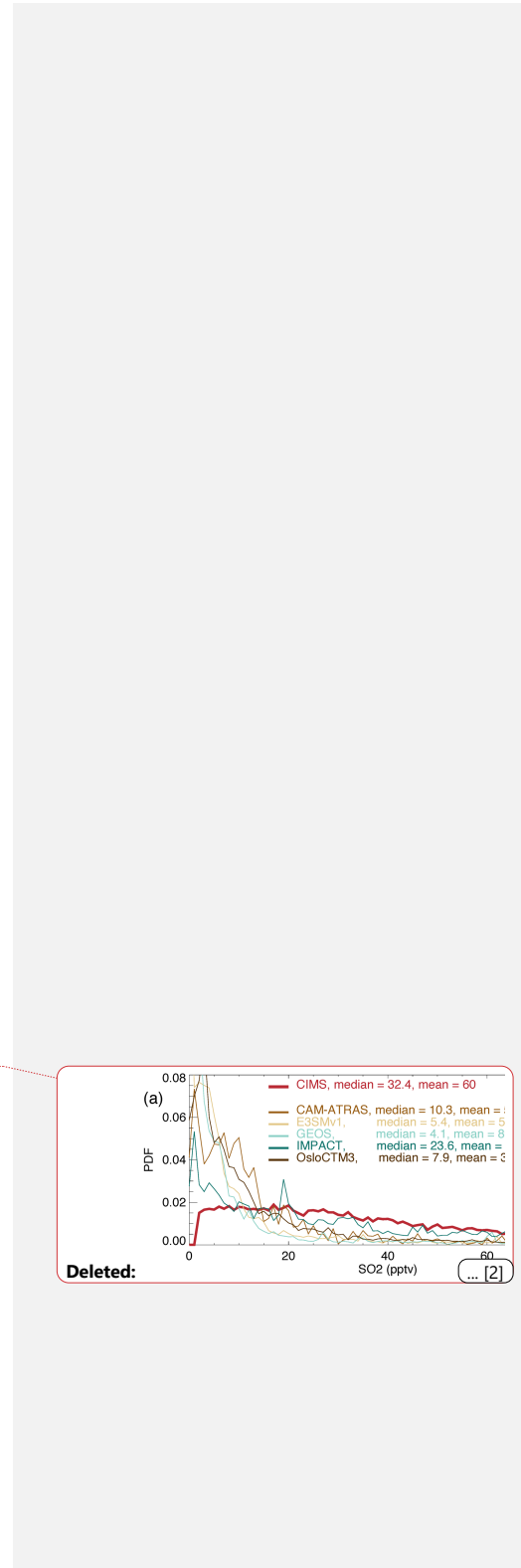


Figure 2. SO₄ probability density functions (PDF) and its statistical values shown by box-and-whisker for the four ATom deployments. All data (AMS in red, PALMS in grey, and five model simulations in other colors) are sampled at 10-s points. Statistical values are calculated when measured values are above the detection limit (DL). Statistical values include the range of the data from minimum to maximum, the three levels of the 25th, 50th (median), and 75th percentiles in the box, and the filled circle for the mean.

1524
1525
1526
1527
1528
1529
1530
1531
1532
1533
1534
1535
1536
1537
1538



1540

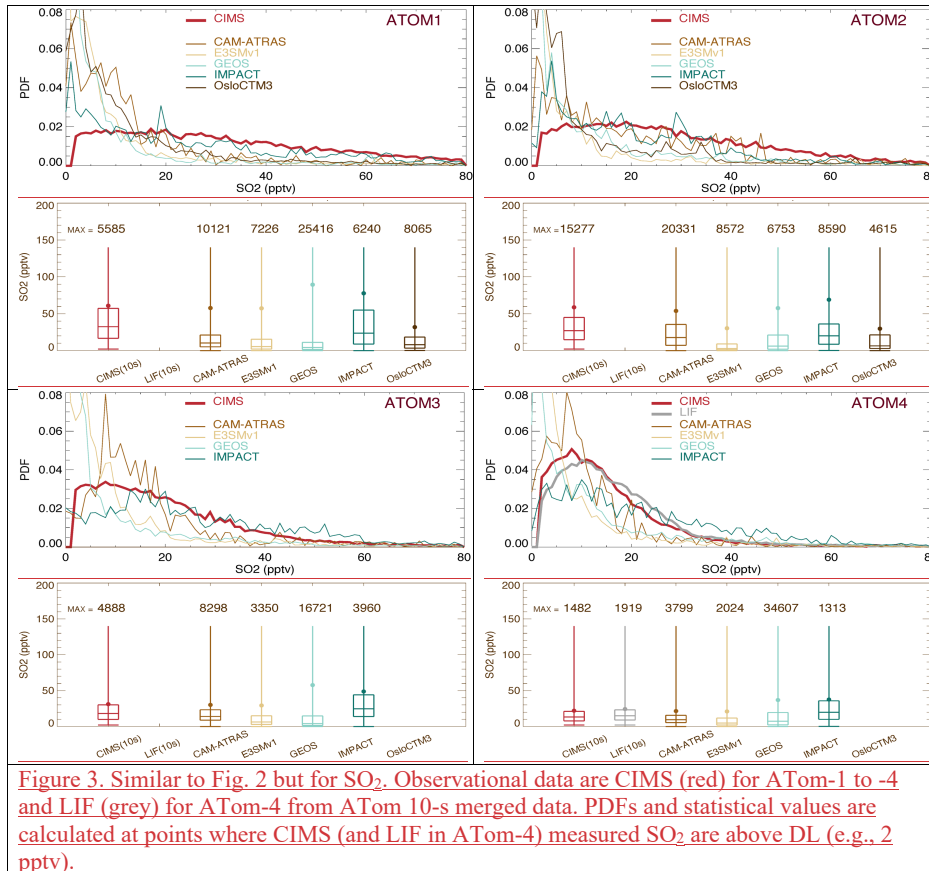
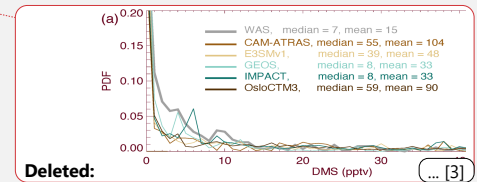


Figure 3. Similar to Fig. 2 but for SO₂. Observational data are CIMS (red) for ATom-1 to -4 and LIF (grey) for ATom-4 from ATom 10-s merged data. PDFs and statistical values are calculated at points where CIMS (and LIF in ATom-4) measured SO₂ are above DL (e.g., 2 pptv).

1541
1542
1543
1544
1545
1546
1547
1548
1549
1550
1551
1552



Deleted:

[3]

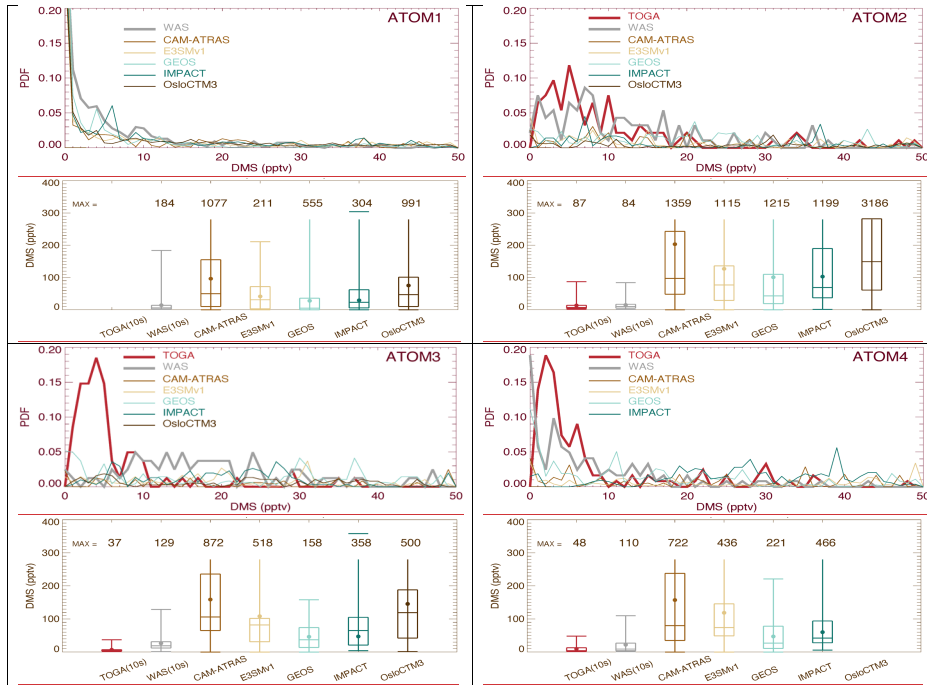


Figure 4. Similar to Fig. 2 but for DMS for ATom-1 to -4. The original data reported by TOGA (e.g., 35-s) and by WAS (e.g., ~60-s) have also been converted to 10-s frequency. Data included in PDF and statistical analysis are on 10-s points where DMS measured by both TOGA and WAS are above DL (i.e., 1 pptv).

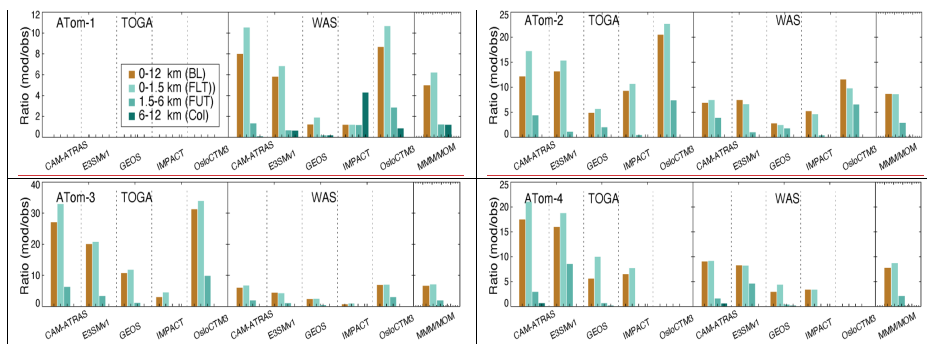


Figure 5. Ratio of DMS median values between model simulation and observation for four ATom deployments. Ratio analyses are performed on four vertical ranges as shown in four colors (see legend in ATom-1). The last column “MMM/MOM” refers to multi-model median to multi-observation median.

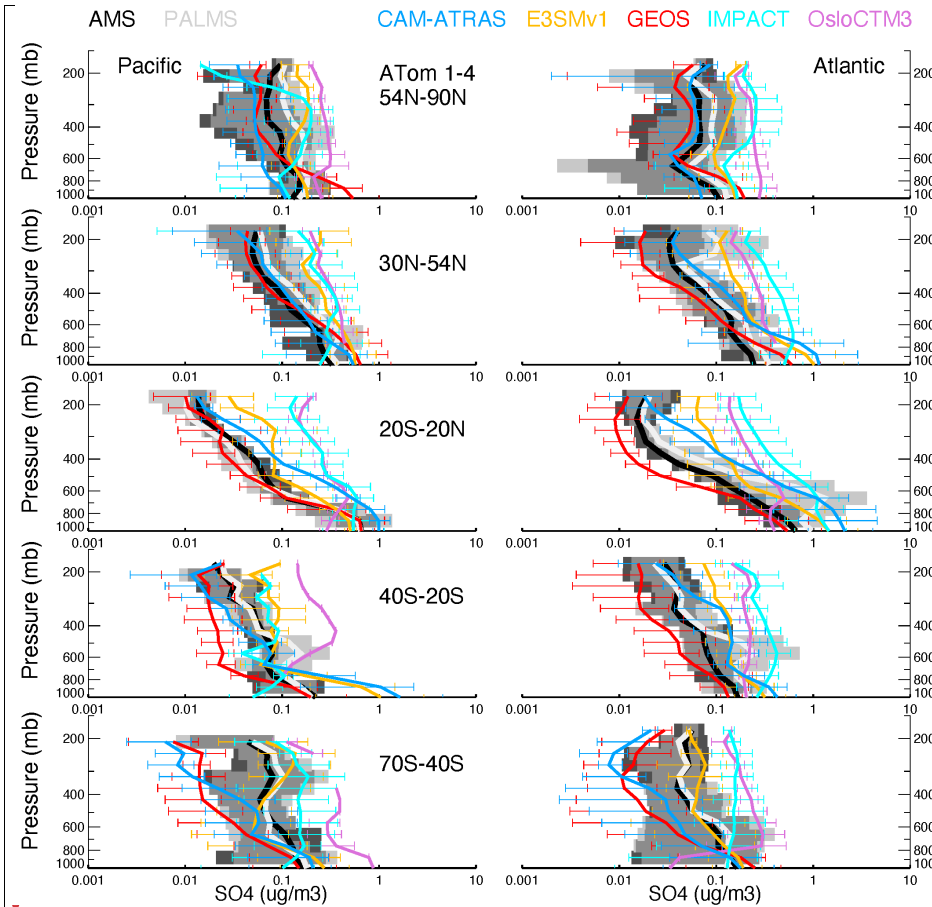


Figure 6. Observed and modeled vertical profiles of SO₄ in 1-km vertical bins averaged for four ATom deployments (lines) and variation across the four AToms (shaded area for measurements and horizontal bars for simulations). ATom measurements are shown in black (AMS) and light grey (PALMS) while model results are shown in other colors. Comparisons are conducted only when both observational measurements above detect limitation are available. Comparisons are separated into five latitude bands from the Northern to the Southern Hemisphere, and into Pacific and Atlantic Basins.

1555
1556
1557
1558
1559
1560

Deleted:
Deleted: 5

Deleted: n
Deleted: s
Deleted: h

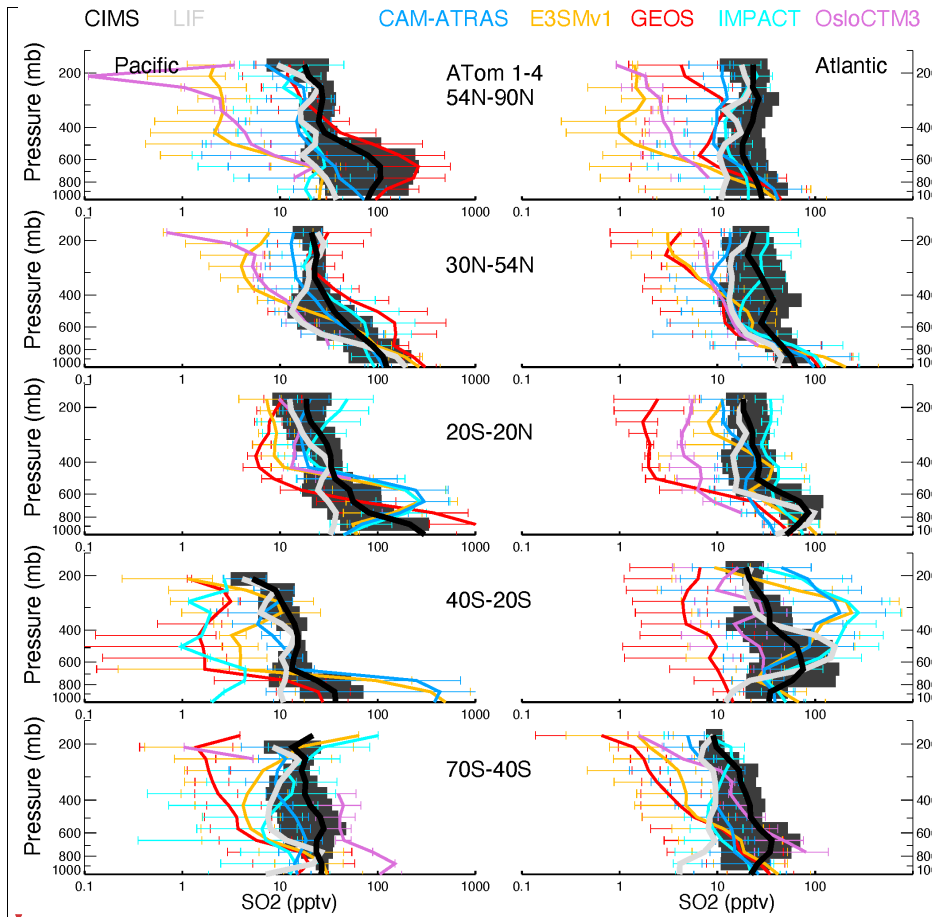
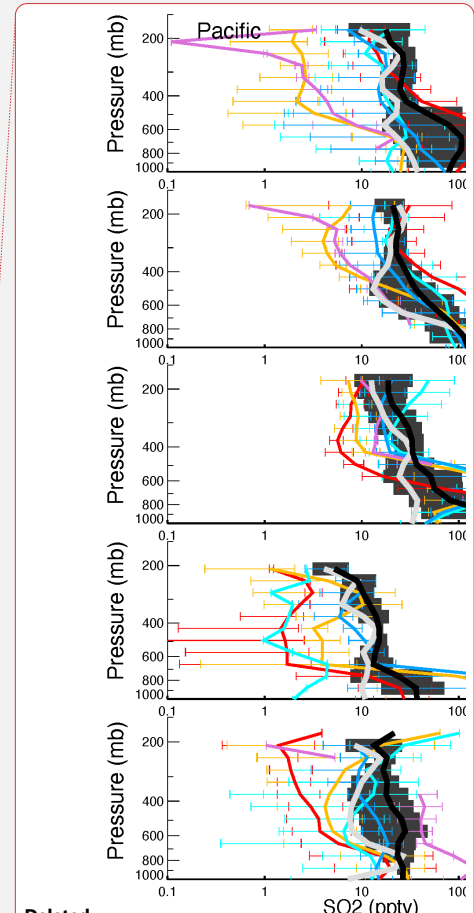


Figure 7. Similar to Fig. 6, but for SO₂. Note LIF (light grey) was deployed only in ATom-4.



Deleted:

Deleted: 6

Deleted: 5

1566
1567
1568
1569
1570
1571
1572
1573
1574
1575
1576

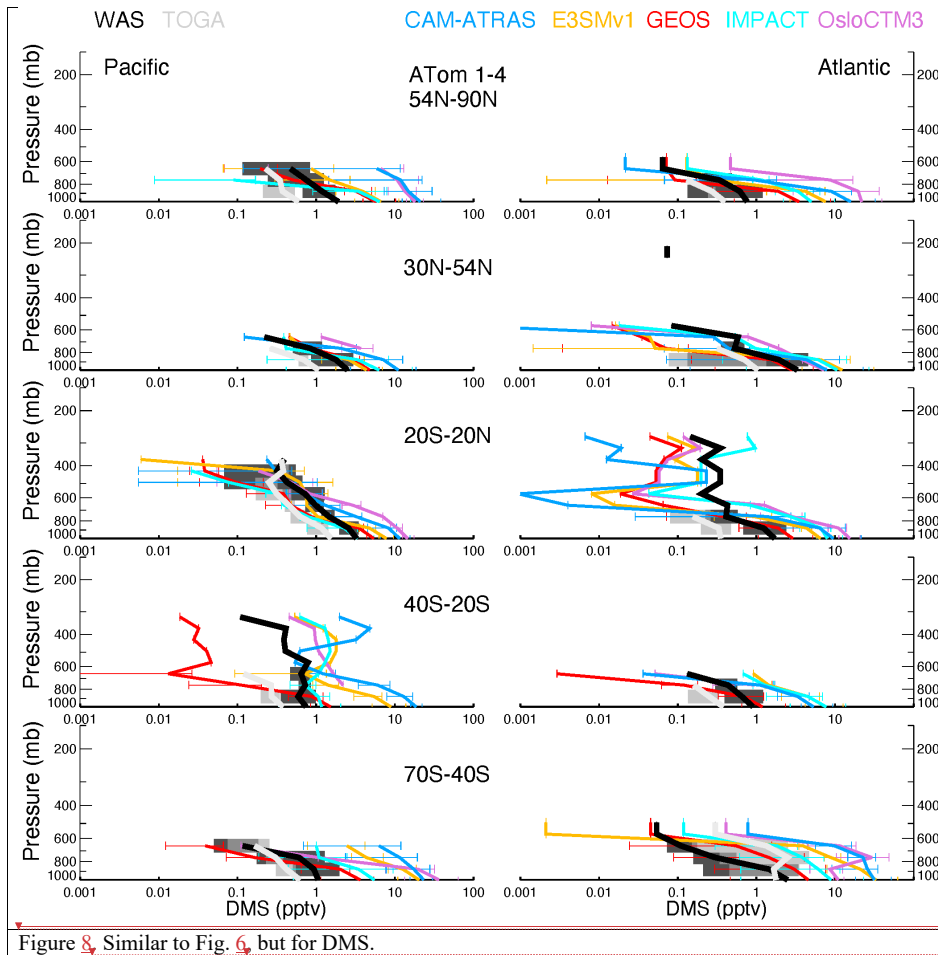


Figure 8. Similar to Fig. 6 but for DMS.

Deleted:
Deleted: 7
Deleted: 5

1580
1581
1582
1583

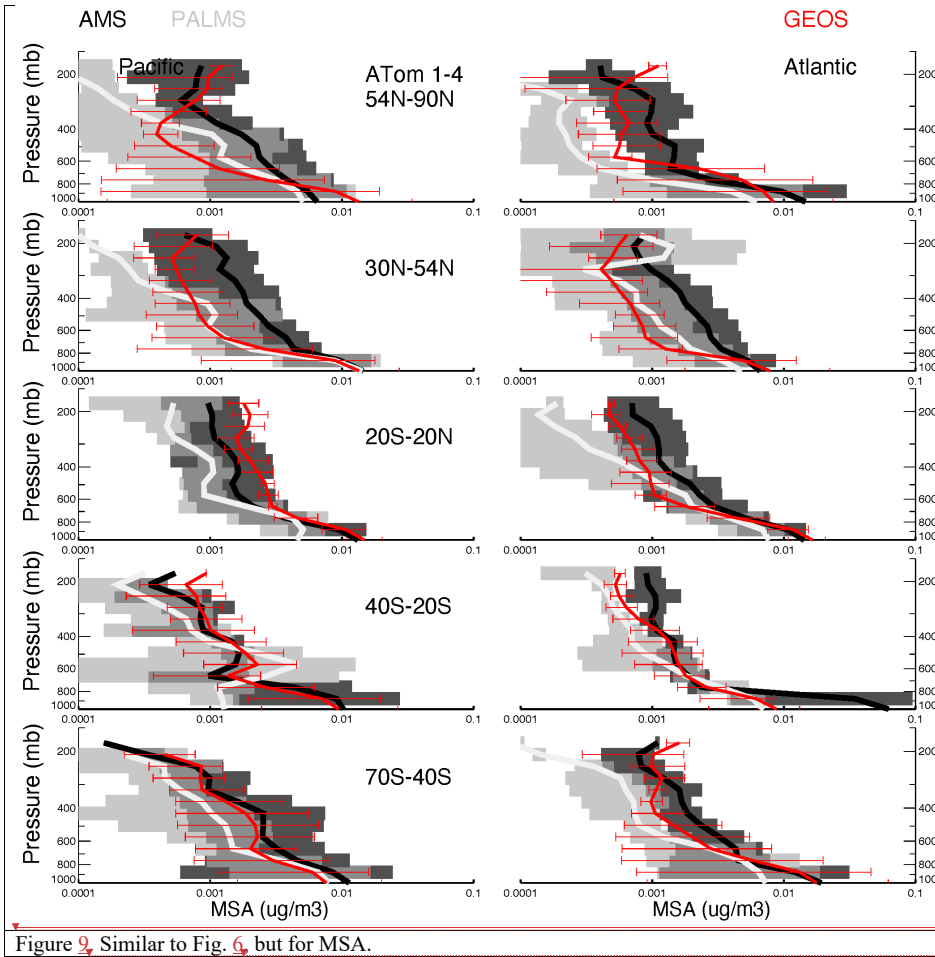
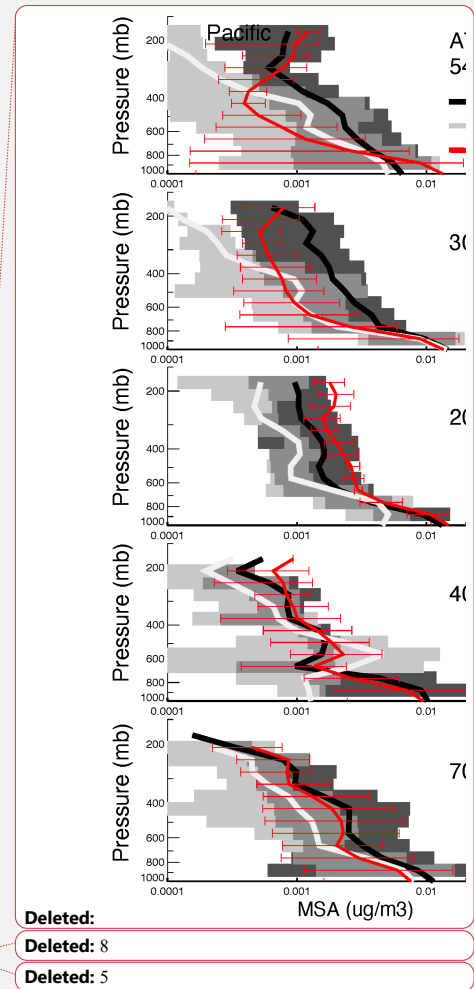


Figure 9. Similar to Fig. 6, but for MSA.



1587
1588
1589
1590
1591
1592
1593

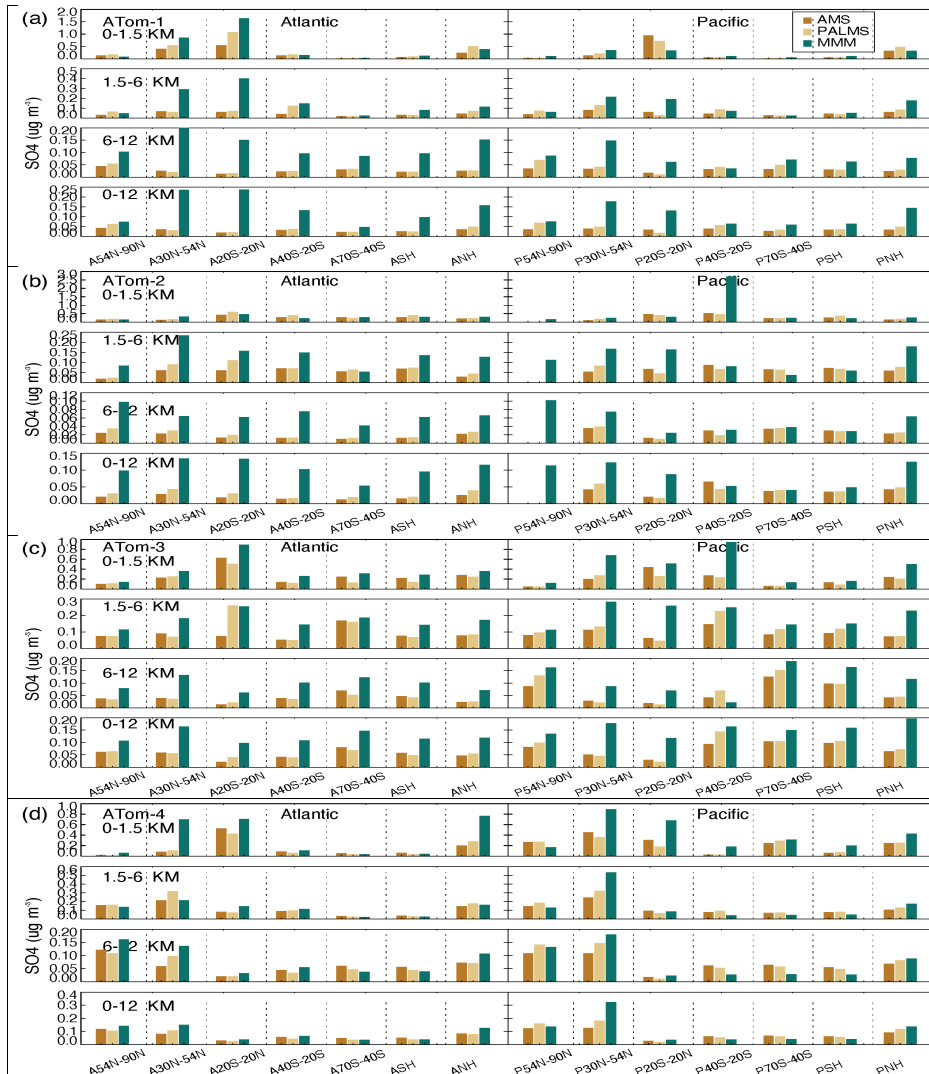


Figure 10. Median SO₄ concentrations from two measurements (AMS orange and PALMS yellow) and multi-model simulation (green) at seven latitudinal bands (including SH and NH) and four vertical layers (i.e., 0-1.5 km, 1.5-6 km, 6-12km, and 0-12 km) over Atlantic and Pacific oceans for four ATom deployments (a-d).

Deleted: 9
 Deleted: red
 Deleted:

1597
 1598
 1599

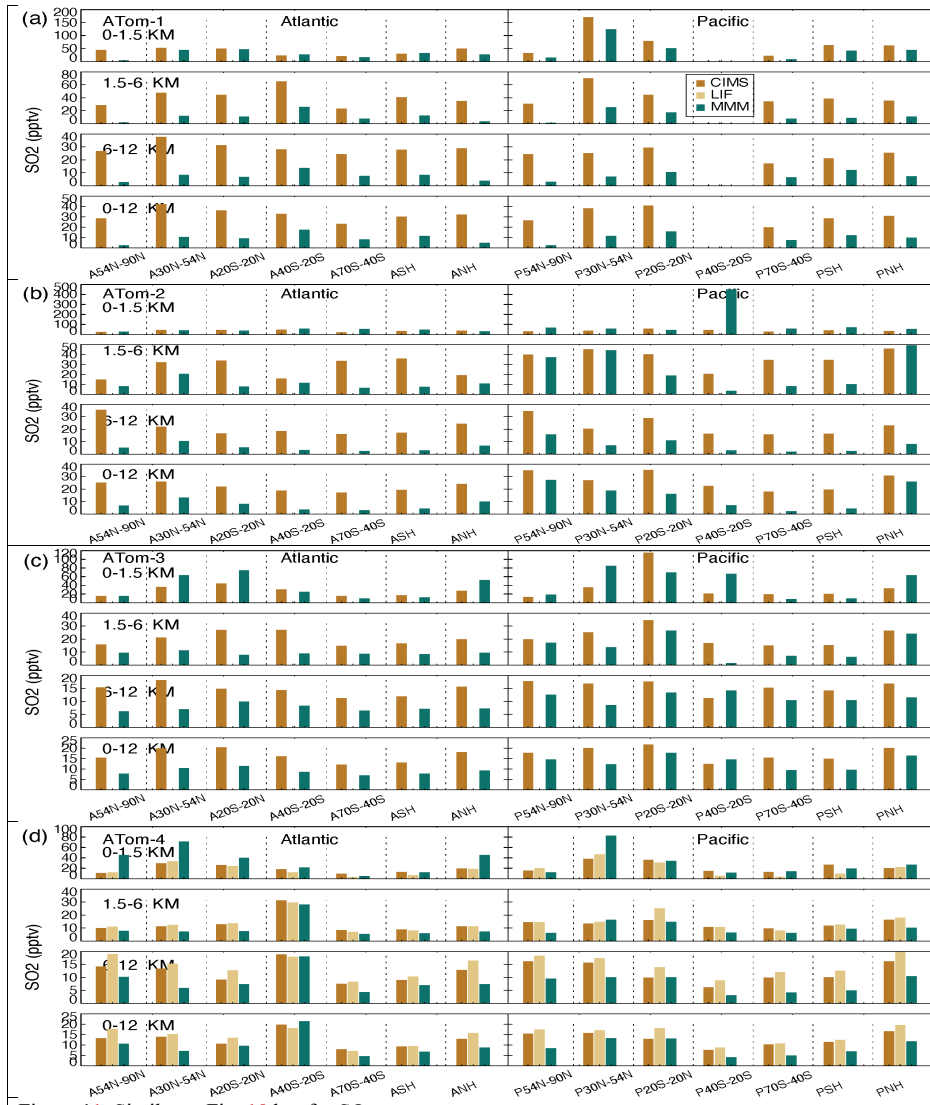


Figure 11. Similar to Fig. 10 but for SO₂.

Deleted: 0

Deleted: 9

1603
1604
1605
1606
1607

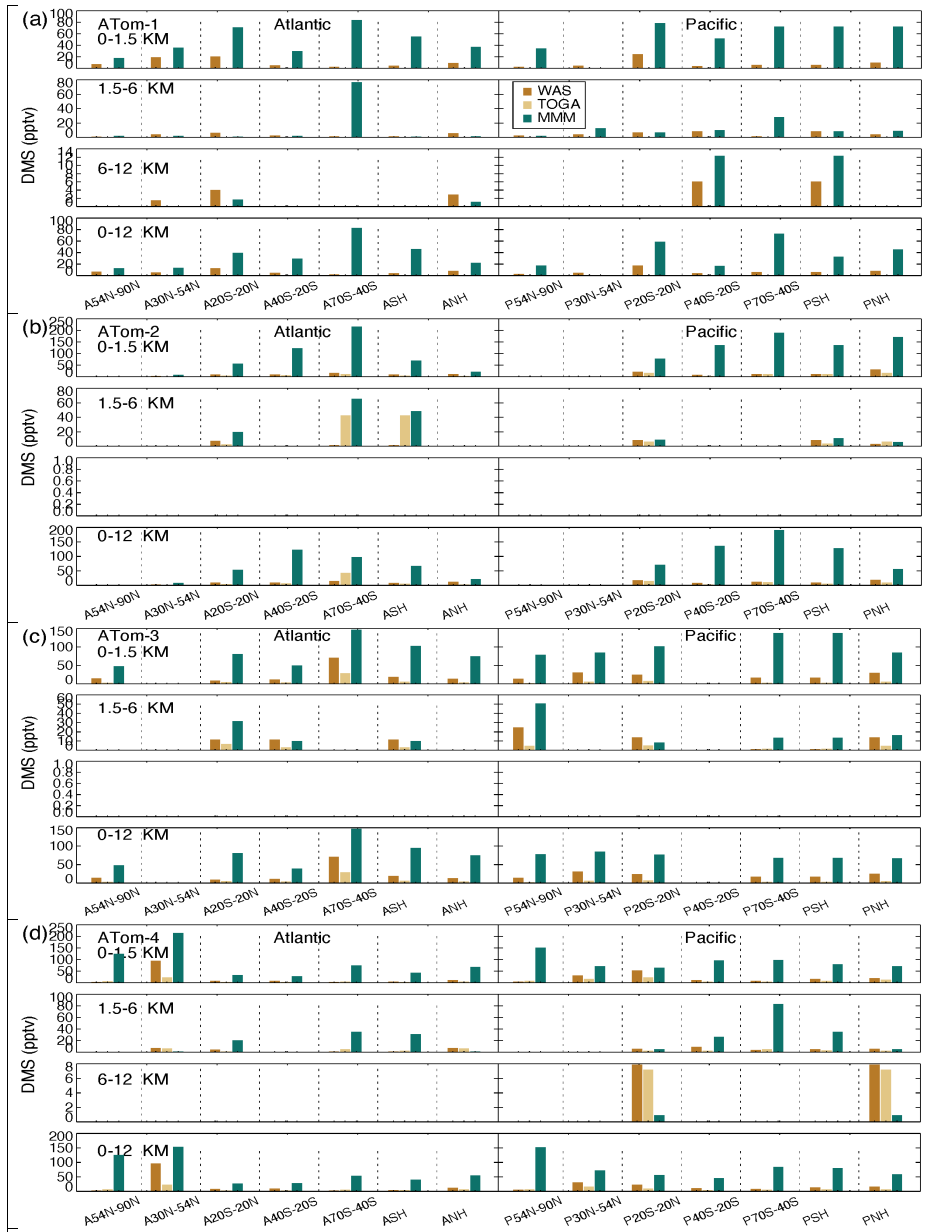


Figure 12. Similar to Fig. 10 but for DMS.

1610

Deleted: 1

Deleted: 9

1613

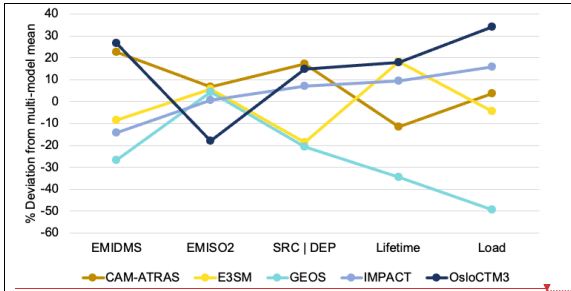
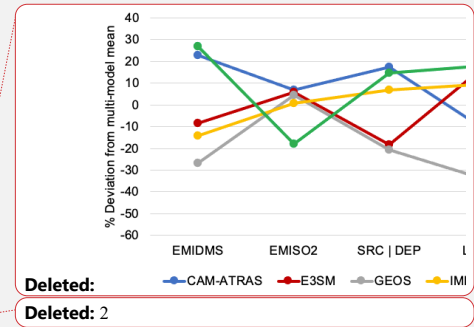


Figure 13. Deviation from multi-model mean for key budget items in sulfur study include DMS emission, SO₂ emission, sulfate source or total deposition, sulfate lifetime, and total sulfate atmospheric mass load.



1614
1615

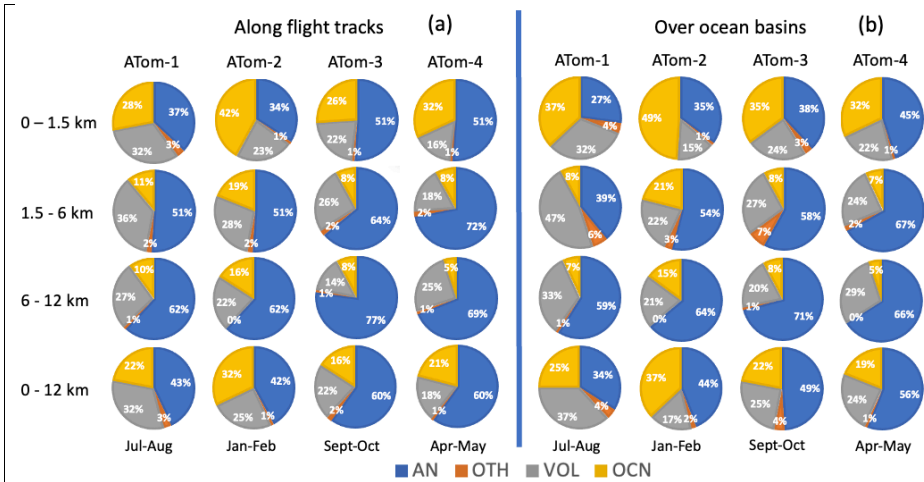
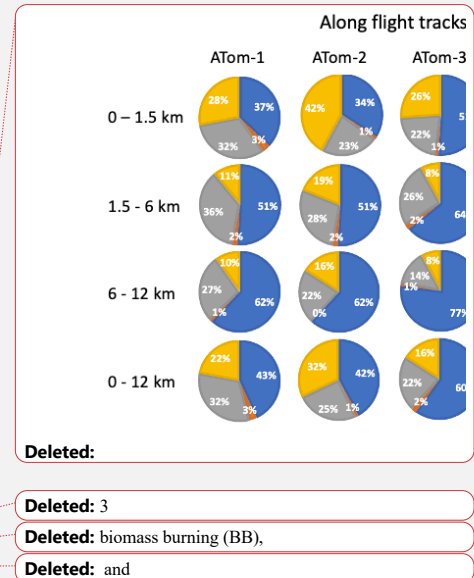


Figure 14. Source origins in percentage (%) for aerosol SO₄ along flight tracks (a) and for a wide oceanic area (b) based on the results from GEOS. Source origins are identified as anthropogenic (AN), volcanic (VOL), oceanic (OCN), and other sources (OTH). Ocean basins include shaded region shown in Fig. 1.



1616

**Page 29: [1] Deleted Bian, Huisheng (GSFC-614.0)[UNIVERSITY OF MARYLAND BALTIMORE CO] 11/1/23
7:43:00 PM**

**Page 30: [2] Deleted Bian, Huisheng (GSFC-614.0)[UNIVERSITY OF MARYLAND BALTIMORE CO] 11/1/23
7:45:00 PM**

**Page 31: [3] Deleted Bian, Huisheng (GSFC-614.0)[UNIVERSITY OF MARYLAND BALTIMORE CO] 11/1/23
7:45:00 PM**